ABSTRACT

HYDRICK, AARON EUGENE. Thin Film Shape Sensing: The Development of an Integrated Flexible Thin Film Temperature-Compensated Strain Sensing Array. (Under the direction of Angus I. Kingon)

The purpose of the Thin Film Shape Sensing project was to develop an array of temperature-compensated strain sensors to be used as a shape sensing array capable of detecting changes in the shape of surfaces such as airfoils. In the case of morphing surface technology, this type of sensor array would provide the necessary feedback to remotely sense and control the shape of the surface.

This project has employed the use of NiChrome (80% Ni, 20% Cr) strain gages and NiChrome/Platinum paired element thermistors for temperature sensing. The sensors were initially developed on DuPont Kapton® and later on a different DuPont polyimide substrate provided by Cirexx®. Three prototype arrays have been developed and tested for basic functionality. The first prototype was designed, built and tested. Basic sensor functionality (electrical response to strain and temperature) was shown. After a substantial redesign including sensor size reduction and processing refinements intended to improve the sensor properties, a second array was produced and tested, showing improvements in sensor performance and overall array functionality. A third and final prototype was fabricated at ½ the original linear dimensions of the second array to show scalability of the array's features. Overall, this prototype was also functional with sensor properties similar to the full-size prototype.

THIN FILM SHAPE SENSING: THE DEVELOPMENT OF AN INTEGRATED FLEXIBLE THIN FILM TEMPERATURE-COMPENSATED STRAIN SENSING ARRAY

by

AARON EUGENE HYDRICK

A thesis submitted to the Graduate Faculty of
North Carolina State University
in partial fulfillment of the
requirements for the Degree of
Master of Science

Materials Science and Engineering

Raleigh

2006

APPROVED BY:

_____

Chair of Advisory Committee: Dr. Angus Kingon
Professor of Materials Science and Engineering

_____

Dr. Ronald Scattergood
Director of Graduate Programs

_____

Dr. Herbert Eckerlin
Professor of Mechanical & Aerospace Engineering

DEDICATION

This thesis and the research it represents is dedicated to the all of the people in my life who believed in me, especially when I did not believe in myself – these would include, but not be limited to: my parents, my family, my friends, my teachers and my wife. Without their support, guidance and prayers – I could not have succeeded as I have!

BIOGRAPHY

Aaron Hydrick was born on February 8th 1971 in Orangeburg SC to Bernard and Evelyn Hydrick and is the youngest of three children. He has been blessed with curiosity from as early in his history as he can remember. His curiosity and talents are in no way limited to the sciences, though he has chosen to pursue the sciences in education. He has been a member of several performing ensembles, vocal and instrumental. He is an accomplished jazz musician who has performed and composed. He holds a love of food and cooking, as well as biking, water and snow skiing, drawing, writing – both poetry and prose, rocketry, reading, anything related to science fiction, truly hot peppers, racquetball and big band music. He enlisted in the Naval Nuclear Propulsion Program at age 21 in May of 1992 and served for 6 years as a nuclear reactor operator. While in the Navy he discovered that he loved to teach – a talent which he would revisit and refine during his tenure at Alfred University as an undergraduate student in Ceramic Engineering and Electrical Engineering. At Alfred, he would found a rocketry club and become Co-Captain of the University rescue squad and among other things, he would meet his wife. After marrying on January 3rd 2004, he began work on his MS degree in Materials Science and Engineering at North Carolina State University. His degree program is now complete and he eagerly seeks whatever challenges God may place before him in the days to come.

ACKNOWLEDGEMENTS

I would like to thank the following people for their help in this research work.

- Dr. Angus Kingon – for his support, patience and guidance throughout my masters work
- Dr. Ronald Scattergood and Dr. Herbert Eckerlin – for taking the time to review my work and serve on my thesis committee
- The U.S. Air Force – for providing funding for the research
- Qor-Tek – for their support and collaboration on this project
- Dr. Jon-Paul Maria – for allowing the use of his laboratory and equipment as well as for his technical help and advice
- Dr. Daniel Lichtenwalner – for his patience and guidance during this research
- Sutherland Products – for the gracious donation of their superior critical cleaning agent: "Charlie's Soap®"
- Joan O'Sullivan – for her expert guidance and instruction in the use of the clean room equipment and processes without which this research would not have been possible
- Jen Hydrick – My Wife, for her unending patience and support throughout these past two years of seemingly endless classes, projects and reports!

TABLE OF CONTENTS

LIST OF TABLES

LIST OF FIGURES

INTRODUCTION

This thesis presents the development of a flexible thin film temperature compensated shape sensing array. The fabrication of a flexible large-area strain sensing array with integrated temperature compensation is one concept innovation incorporated in this research. The purpose of such an array of integrated sensors would include such applications as morphing wing technology, which would replace conventional control surfaces (ailerons, elevators, rudders, etc.) with the ability for an entire airfoil to morph according to the control needs of the aircraft. Figure 1 illustrates the concept of wing morphing as a control surface.

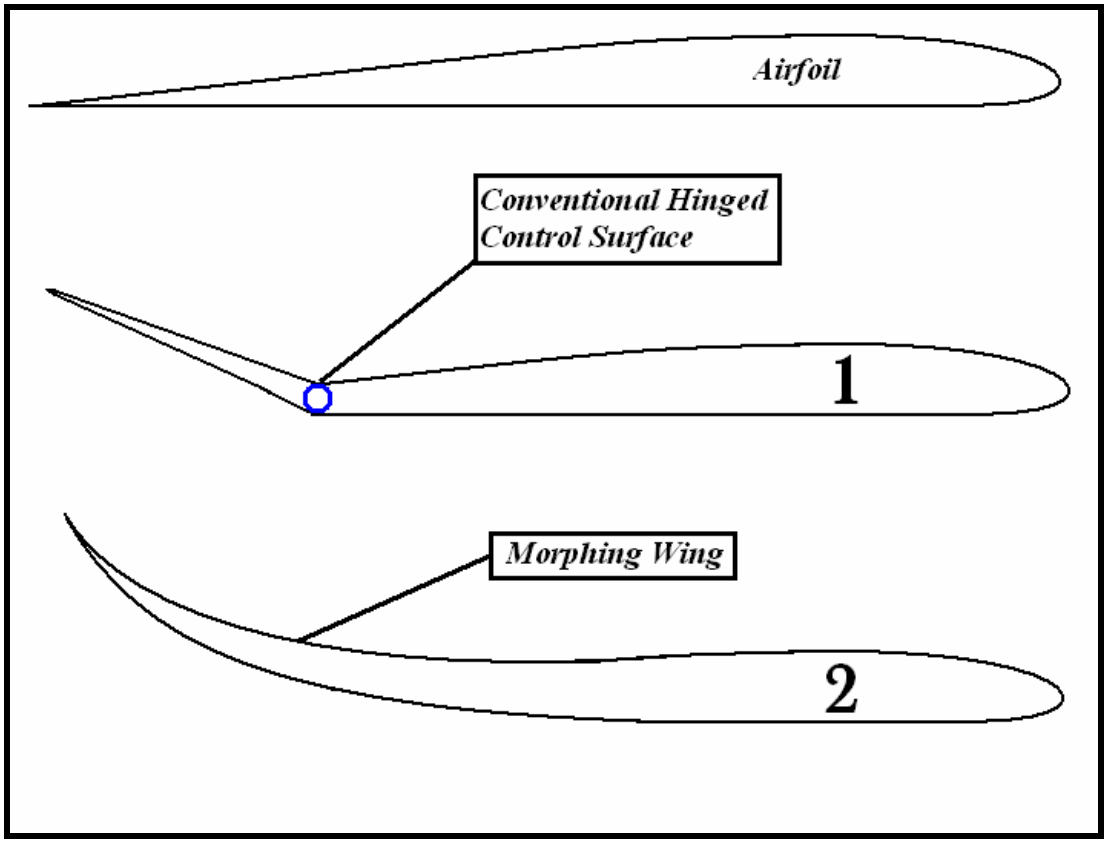

Figure 1: Morphing Wing Technology as Replacement for Conventional Control Surface

This type of morphing technology would also replace other hinged wing configuration motions such as the variable dynamic swept-wing of the now-retired F-14 Tomcat. In order to achieve the level of precise control of a morphing wing required for flight, rapid, accurate feedback is critical (Figure 2).

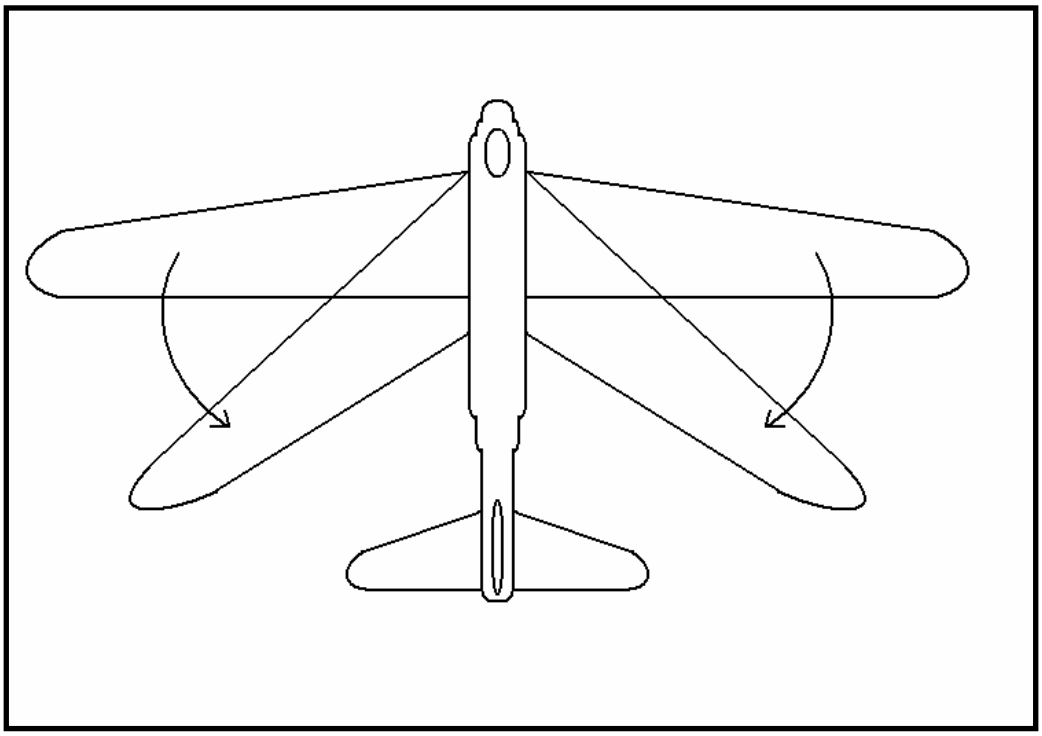

Figure 2: Morphing Wing Technology as Means of Altering Wing Configuration

Control of such an aircraft would require the ability to tile sensors over the entire wing area and that they provide accurate feedback of strain (i.e. shape) over the bulk of the wing area. The need for temperature compensation is due to the construction of the strain sensing elements. The type of strain gage referred to in this research is essentially a length of wire, whose resistance is subject to variance not only with respect to strain, but also temperature. In creating a shape sensing array that is subjected to the thermal extremes and variances experienced by an aircraft surface, one must also consider the morphing technology as well. The "morphing" effect is most likely driven by piezo

actuators which will in turn generate localized heating. For these reasons, temperature compensation must be integrated into the array. The sensors will operate on the principle of change in resistance as a function of change in temperature and change in length, so the electronics related to sensing as well as the general sensor design are identical for the strain gauges and the resistance temperature detectors (RTD). Kapton® was chosen as the substrate material both for its flexibility, and because of its thermally and chemically robust nature. One unique design aspect is the use of two resistive sensor materials, each with different strain and temperature responses. To achieve accurate strain sensing in the plane of the array, a 3-element "strain rosette" pattern was chosen, to be fabricated from NiChrome (NiCr). NiCr (80%Ni, 20%Cr) was an ideal choice as the strain sensing element because it has a near-zero temperature coefficient of resistance (TCR). Temperature compensation is provided by using a Platinum element (a strain gauge design similar in size and shape to the NiCr sensors) – at least one temperature compensating Pt sensor accompanies each strain rosette. Pt was chosen as the temperature sensing material rather than strain sensing because even though it has higher strain sensitivity than NiCr it has a very well defined linear response to temperature over a wide range of temperatures. Key sensor layout design aspects were: 1) the placement of Pt and NiCr in parallel pairs to separate T and ε; and 2) placement of NiCr sensors in rosette patterns to determine strain magnitude and direction. (Note: In the first prototype array, the Pt/NiCr RTD paired elements were separate from the rosette, in the second prototype the NiCr portion of the paired element is actually part of the rosette.) One design goal related to initial sensor layout was for all sensor elements to have 100Ω of

resistance (a standard for RTD sensors) – this would allow for the simplification of sensing circuitry and help to minimize power consumption.

Having discussed the separate sensing elements and material selection, the concept of paired sensing elements should be addressed separately. The idea of separately measuring both strain and temperature in the same sensing array at essentially the same physical location involves collinear placement of the paired elements in very close proximity to one another. In so doing, the different material properties of each sensor allow the values of both strain and temperature to be determined by de-convoluting the signal information by using unique simultaneously solved equations containing the strain sensitivity and temperature sensitivity as constant, known values.

We have created three array prototypes. The first allowed a determination of basic sensor properties and fabrication techniques. The initial array was fabricated on a 6"x 6" sheet of 75μm DuPont Kapton® and was a rectangular array of 36 elements in a 4"x 4" active area. The original array design was intended to address sensors via a modified "row and column" address format which included a modified three-lead configuration for more accurate resistance measurements. Due to problems with the design of the electrical interconnects, a complete redesign of the sensor layout was proposed for a second array prototype. The substrate for this prototype, provided by Cirexx®, is a 6"x 6" DuPont Pyralux® polyimide patch with prefabricated Cu connection lines. This prototype patch, demonstrates the feasibility of all original aspects of the project. We show that the Pt and NiCr sensors have different temperature and strain responses, thus the separation of thermal effects using paired NiCr and Pt elements is

proven. We also show in a third prototype that scaling down the sensor size by a factor of 2 gives nearly identical results, thus proving the ability to scale sensor density.

Flexible large area sensor arrays are a critical component of future 'smart' systems intended to provide immediate feedback of component conditions during operation. For shape-changing surfaces, flexible arrays of strain sensors with temperature compensation elements would allow an accurate, rapid feedback response to any shape change with virtually no error due to localized heating – this is a must for applications such as aircraft control surfaces or morphing wings.

Sensor arrays were fabricated on polyimide sheets, using DC magnetron sputter deposition of sensors and Cu conductor layers, and patterned using photolithographic techniques adapted to the processing on polyimide sheets. Magnetron sputter deposition of each material (Pt, NiCr, and Cu) was performed in order to determine conditions for obtaining acceptable uniformity across a 6" tile, and to find film resistivity and TCR values for these films. A film thickness uniformity of ±10% was achieved for Pt deposited over a 6" diameter area, which was sufficient to fabricate and test the prototypes. Similar testing was performed to achieve acceptable film properties with regard to resistivity and stress.

An initial sensor array prototype of simple design and relatively large sensor sizes was used to aid in determining optimal processing conditions for array fabrication. The prototype array allowed testing of the materials used for the sensors, the "strain rosette" concept, and included a modified "three-wire" resistance measurement configuration to help increase the accuracy of the resistance measurements. This array was also

instrumental in showing the feasibility of using a liquid, photodefinable polyimide as a process step to insulate metallization layers in flex circuit development.

After assessing the design problems with the original prototype array, a second array was planned and developed to include several improvements suggested at the meeting with the Air Force, QorTek and NCSU in Dayton Ohio. This array includes the following specific features:

- Linear sensor dimensions ½ that of original array – occupying ¼ the original surface area;
- Increased number of sensors on the same 6"x6" Kapton® patch;
- Sensor-on-sensor design utilizing the photodefinable polyimide to allow the temperature sensor to be placed ~5μm directly above one of the strain sensors.

The second array consists of 48 sensors and 64 leads. The sensors are grouped in sets of eight, with each group containing two three-element NiCr rosettes and two Pt temperature sensors. Each sensor has an individual address lead and each group has two common leads to complete the three-lead configuration. There are six groups of eight sensors (60 leads), plus four leads that address six NiCr and six Pt test pads in the center of the array. The center pads are intended to provide a means of measuring and/or compensating for the contact resistance between Cu and each of the two metals. The NiCr pads in the center are electrically in parallel, so as to minimize error due to exceptionally high contact resistance on one or two pads. The Pt pads are configured in the same manner as the NiCr. The active area of the 48 element array is less than two square inches.

LITERATURE REVIEW

STRAIN SENSORS

The measurement of strain as a function of electrical resistivity was first discovered by Lord Kelvin in 1856 – Lord Kelvin observed that resistance of metal wires varied with applied axial strain[1]. Early un-bonded wire strain gages were used in conjunction with Wheatstone bridge circuits, and were not easy to use. The first bonded, metallic wire-type strain gage was developed in 1938[2]. This type of gage is generally constructed by bonding a metal foil to a polymer backing or substrate such as Kapton®, a DuPont polyimide. The smallest commercially available bonded foil strain gages are the KFRS series, at 1.1mm in length[3] but state of the art technology has created strain gages as small as 0.2mm. Accurate determination of surface strain requires the use of strain sensors in a rosette pattern, since the direction of strain may differ with sensor location and various loading conditions. We have chosen a planar rectangular rosette pattern as in Figure 3 for strain sensing.

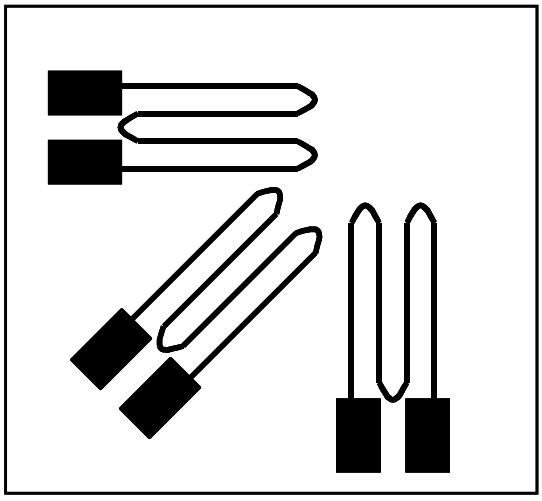

Figure 3: Schematic representation of rectangular strain sensor rosette pattern

Each rosette of 3 sensors then allows determination of strain and strain direction at a given location. More details related to this sensor configuration can be found in the text by Young *et al*[4]. The technique for extrapolating directions elements of strain from this sensor configuration is based on the applications of a few simultaneous equations and the principles of Mohr's Circle. Please refer to Figures 4 and 5 in conjunction with the following explanation. For the specific case of the rectangular (or 45º) configuration shown in Figure 4, the sensors a, b & c correspond to the following angles: $\theta_a = 0º$, $\theta_b = 45º$, $\theta_c = 90º$. In this case:

$$\varepsilon_x = \varepsilon_a$$

$$\varepsilon_y = \varepsilon_c$$

$$\gamma_{xy} = 2\varepsilon_b - (\varepsilon_a + \varepsilon_c)$$

After the determination of ε_x, ε_y and γ_{xy} it is possible to then apply the principles of Mohr's Circle (as indicated in Figure 5) to determine the principle in-plane strains as measured by the gages. A full and complete explanation of this type of calculation is given in the text by R.C. Hibbeler[5].

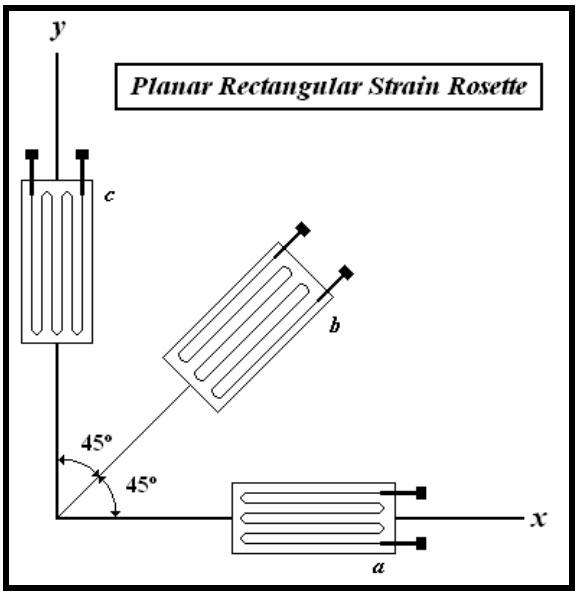

Figure 4: Basic Planar Rectangular Strain Rosette

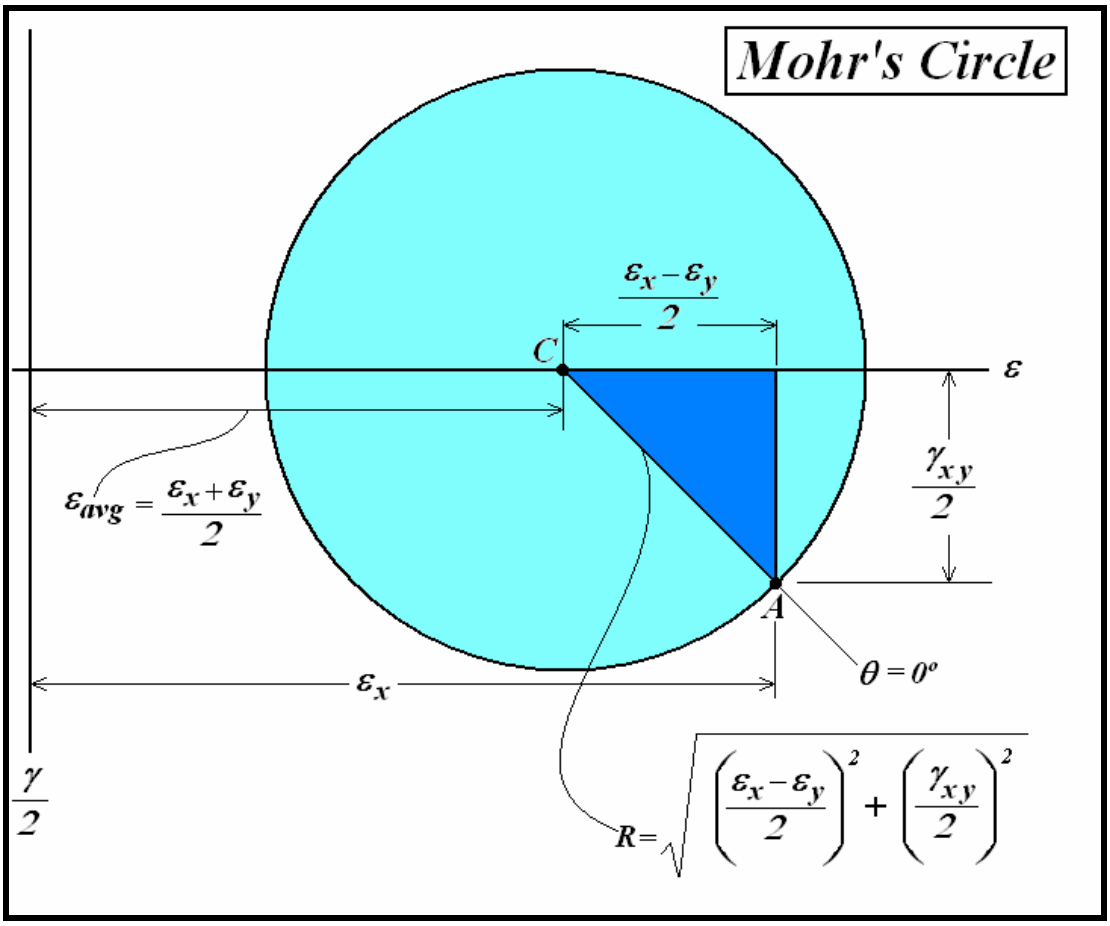

Figure 5: Mohr's Circle Diagram and Equations

For NiCr, the ratio of strain sensitivity to temperature coefficient is 15 times higher than for Pt, so that temperature effects will not significantly affect strain readings[6] (not accounting for thermal expansion coefficient differences of the sensor patch and the material to which it is affixed). The measurement of strain using an electronic strain gage is facilitated by understanding the strain response or *gage factor* (GF), which is described in the following equation, where R_f is the final measured resistance, R_o is the initial measured resistance and L_f and L_o are the final and initial measured lengths of the object being strained. Also note that the denominator of the GF equation is in fact strain (ε).

$$GF = \frac{\left(\frac{R_f - R_o}{R_o}\right)}{\left(\frac{L_f - L_o}{L_o}\right)} \qquad GF = \frac{\left(\frac{R_f}{R_o} - 1\right)}{(\varepsilon)}$$

Koch has collected data showing that ultra-fine grained bulk metal are in general higher in stiffness and lower in ductility than bulk metals with larger grain sizes[7]. Koch also states that in general, the Hall-Petch grain-size to yield-strength relationship holds for all but the smallest grain sizes[8].

TEMPERATURE SENSORS

Proper RTD temperature measurement requires the elimination of strain-induced resistance changes. Therefore we have proposed the novel concept of using parallel pairs of Pt and NiCr RTD's to allow the effects of temperature and strain on resistance to be separated. Since the strain gage is also essentially a RTD, the incorporation of similarly sized sensors to operate as paired elements is logical. By combining two sensors of the same basic sized and shape, and mounting them in a coaxial orientation, it is possible to make use of differences in each materials strain and temperature sensitivity to de-convolute the strain and temperature measurements from an array of sensors by simultaneously solving two unique equations involving gage factor and TCR. The RTD was first developed in 1932 by H C Meyers[9]. The measurement of strain using an RTD is facilitated by understanding the thermal response or *Temperature Coefficient of Resistivity* (TCR) denoted as α and sometimes referred to as temperature sensitivity,

which is described in the following equation, where R_f is the final measured resistance, R_o is the initial measured resistance and T_f and T_o are the final and initial measured lengths temperatures. It is important to note that for the purpose of this equation T_o is defined specifically as 0ºC and R_o is similarly defined as the resistance at T_o.

$$\alpha = \left(\frac{R_f - R_o}{R_o \left(T_f - T_o \right)} \right)$$

The NiCr RTD (expected TCR 0.000085 Ω/Ω/^{o}C, strain sensitivity of 2.1) is used to account for the strain-related resistance change from the Pt RTD (expected TCR 0.00385 Ω/Ω/^{o}C, strain sensitivity 6.1). Each RTD is designed to be 100 Ohms, with three-wire sensing. The basic parallel pair sensor design is similar to that shown in Figure 6. Each RTD parallel pair provides for one temperature reading at a given location.

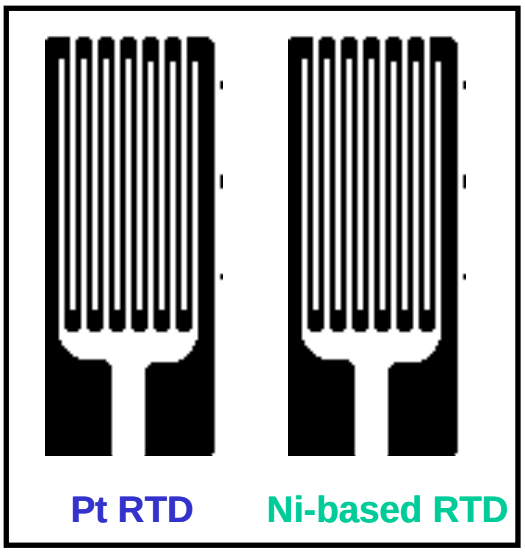

Figure 6: Schematic Representation of Parallel RTD Pair for Temperature Sensing

SIGNAL DECONVOLUTION

To review the equation for temperature coefficient of resistivity given previously:

$$\alpha = \left(\frac{R_f - R_o}{R_o\left(T_f - T_o\right)} \right).$$

This can be re-written as follows:

$$R_T = R_0 \times (1 + \alpha \times T).$$

Again, α refers to the temperature sensitivity to resistance change from a 0°C reference point (R_0), in units of ΔΩ/Ω/°C and R_T refers to the resistance at a given measured temperature T. Also, reviewing the strain sensitivity or gage factor (GF) equation:

$$GF = \frac{\left(\frac{R_f}{R_o} - 1 \right)}{\left(\varepsilon \right)}$$

In this case, a metal undergoing strain (Δl/l, or ε) likewise experiences a resistance change which may be represented by similarly rearranging the above equation as shown below, where R_ε is the measured resistance at a given value of strain (ε).

$$R_\varepsilon = R_0 \times (1 + GF \times \varepsilon),$$

Also the strain sensitivity or gauge factor (GF) is a dimensionless quantity (ΔΩ/Ω/ε).

By evaluating the effects of both temperature and strain, one might expect the effects of small T and ε changes on electrical resistance to scale as follows:

$$R_{(T,\varepsilon)} = R_0 + (R_0 \times GF \times \varepsilon) + (R_0 \times TCR \times T)$$

Note that this equation is referenced to a zero strain, 0°C starting resistance R_0. Thus, with one resistive sensor material, merely obtaining sensor resistive response does not allow strain and temperature to be separately determined.

However, it is possible to make use of a second gage, composed of a different conductor material, and designed having the same physical dimensions and value for R_0 and subject to virtually the same T and ε conditions as the first gauge due to very close proximity placement with collinear strain directions. If in this case these two gages are considered as gage 1 and gage 2, the response of gauges 1 and 2 to the same T and ε conditions can be given by the following equations:

$$R_{1(T,\varepsilon)} = R_0 + (R_0 \times GF_1 \times \varepsilon) + (R_0 \times TCR_1 \times T) \quad \text{and}$$

$$R_{2(T,\varepsilon)} = R_0 + (R_0 \times GF_2 \times \varepsilon) + (R_0 \times TCR_2 \times T)$$

Here, the GF and TCR of the two sensor materials are considered as constants (or known functions of ε or T), and differ from each other. Thus, having 2 sensors fabricated from different materials, the two resistance values allow calculation of the strain and temperature at that given point. Note that each sensor acts as an RTD *and* a strain gauge, but by having two collinear gauges the values can separately be determined without any additional compensation elements. This is a novel approach for determining both strain and temperature concurrently. Slight nonlinearities in TCR or GF would make the

calculation of temperature and strain more complex, but do not negate the applicability of the approach.

SENSOR INTERCONNECTS

The material chosen for interconnects between sensors and to connect the integrated array to off-patch electronics was copper (Cu) since minimizing electrical resistance between sensors was critical. Copper was the logical choice from both a resistivity standpoint and from a processing perspective. Because Cu has a much higher etch rate than either NiCr or Pt, it made the Cu processing considerably easier by allowing a wet-etch as opposed to a liftoff process to be used.

BONDED SENSORS ON FLEXIBLE SUBSTRATES

Companies such as Vishay and Omega to name only a few are currently engaged in the manufacture and commercial sales of both bonded wire/foil strain gages, including integrated strain rosettes of various patterning and several different styles of RTD. The majority of these sensors are manufactured on flexible background materials/substrates such as 25μm or 75μm DuPont Kapton®. Figures 7 and 8 show respectively, a commercially available strain gage and RTD bonded to Kapton®.

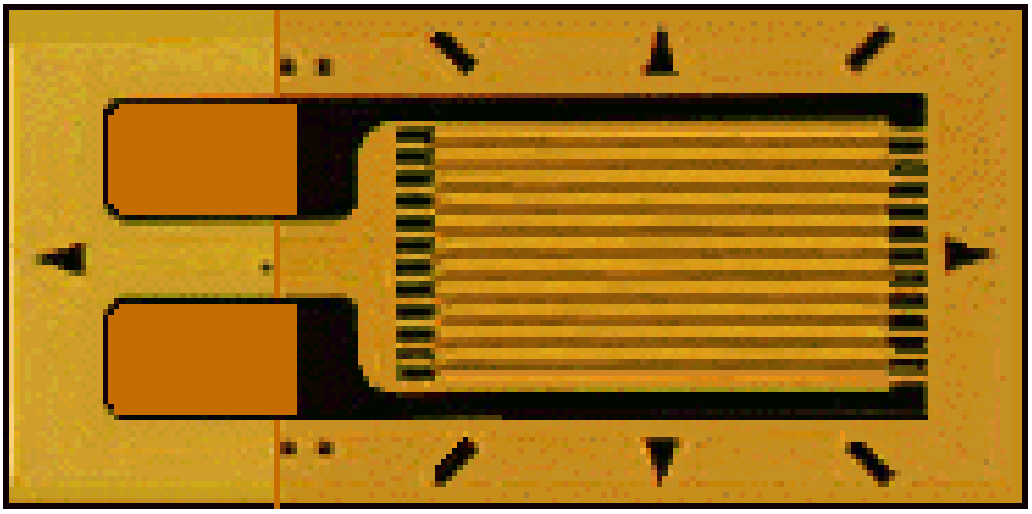

Figure 7: Commercially Available Bonded Wire Strain Gage on Polyimide

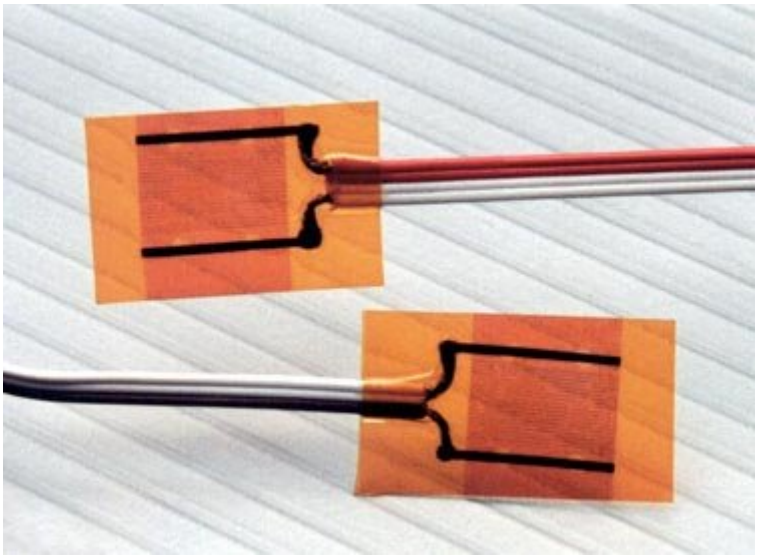

Figure 8: Commercially Available RTD's on Kapton®

THICK FILM COPPER ON CIREXX® POLYIMIDE

Current thick film technology, such as the Cirexx® pre-fabricated patches used in this research use a bonded foil layer of metallization (e.g. Cu) and usually a chemical etching technique to pattern the foils. The patches used in this research have a foil layer ~15μm

thick, which is approximately 10 times thicker than the thin film copper used to pattern the sensor interconnects

RELEVANT PATENT SEARCH INFORMATION

Searches were conducted in an effort to verify that the concepts expressed concepts identified herein as "novel" do not infringe upon any existing patent rights. The searches were for technologies that simultaneously measure both strain and temperature, technologies that integrate anisotropic planar strain sensing capabilities (i.e. strain rosettes) over large areas or in tiled patches and technologies which incorporated 3-dimensional (or z-axis) integration of thin film sensors. Patent searches were conducted on the USPTO website with the following results:

- No relevant patents were found pertaining to integrated strain & temperature sensing arrays
- No relevant patents were found pertaining to integrated large area strain rosette arrays
- No relevant patents were found for 3-dimensionally integrated strain and temperature sensing arrays
- Relevant technology deals with devices developed in 1932 and 1938 (pre-1976)
- According to the USPTO website, patents from 1790 through 1975 are searchable only by Issue Date, Patent Number, and Current US Classification.

After conducting the patent search as described above, it was concluded that the technologies developed as part of this research: including but not limited to integrated strain and temperature sensing, integrated large area strain rosette arrays and

photolithographic patterning of 3-dimensionally integrated strain and temperature sensing arrays are *apparently* novel, but further more detailed investigation is warranted prior to pursuit of patents.

EXPERIMENTAL PROCEDURES

ASSESSMENTS PRIOR TO RESEARCH

- Two metals are required for sensor array to isolate temperature and strain from one another.
- NiChrome has virtually zero temperature coefficient of resistance (TCR) making it an excellent choice for independent strain sensing.
- Platinum has excellent TCR linearity through a large temperature range, making it a logical choice for temperature sensing.

The array prototypes developed during this project included several fabrication steps and preliminary studies. A brief outline of the basic steps taken in development of the arrays is given below followed by a more detailed description of the procedures used.

Process Outline

I. Determine Thickness Uniformity of Sputtered Films

II. Determine Basic RTD and Strain Gauge Properties

III. Design and Fabricate Prototype Array

IV. Test Prototype Array and Review Results – Redesign if Required

In order to determine thickness uniformity, a shadow mask of a basic resistor element was created and several test strips of metal were sputtered onto glass and Kapton®. The test strips were arranged over a 4" x 4" area, and positions of the various test strips within the Magnetron were recorded. The film thickness of the strips in Angstroms (Å) was then measured using a Sloan Dektak II profilometer allowing a film thickness profile for the intended active sensor area to be established. Figure 9 Shows the DC magnetron system used in this research. Figure 10 shows the Magnetron in use.

Figure 9: DC Magnetron System

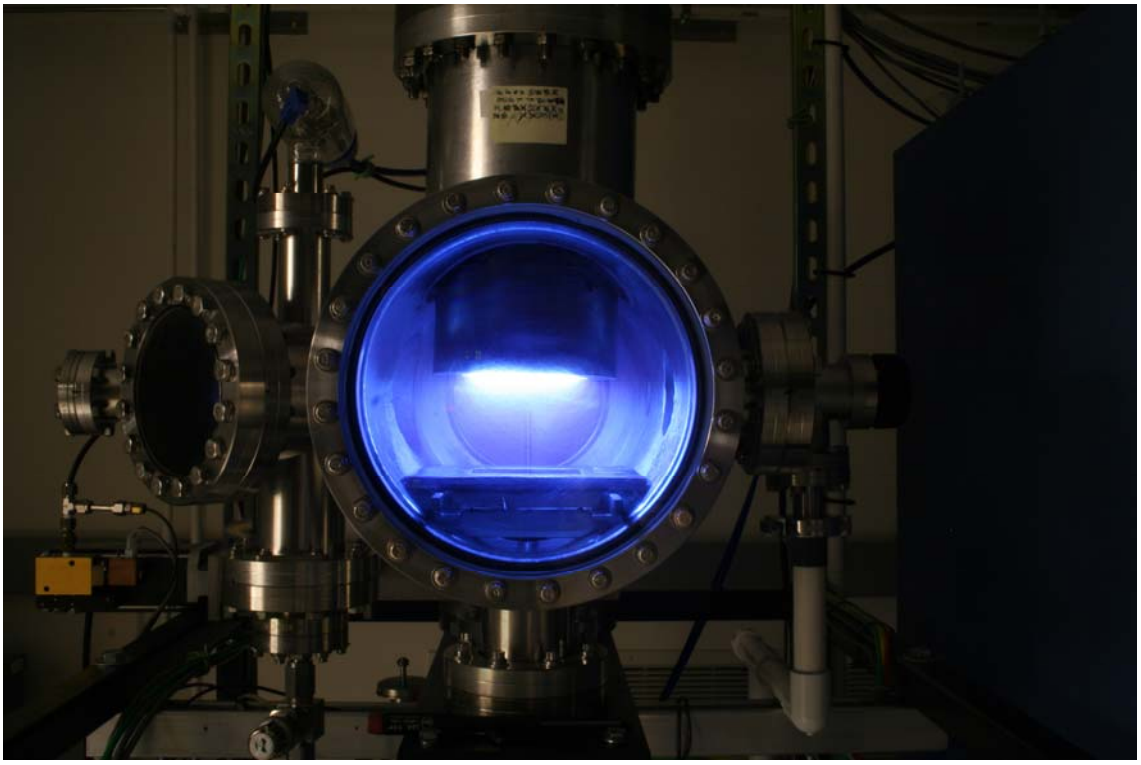

Figure 10: DC Magnetron System in Use

Once acceptable film thickness uniformity was established for the prototype array, more test strips were fabricated on Kapton® and tested for resistivity as well as strain and temperature response. The resistivity was calculated by taking a four-point probe resistance measurement using a high-precision Agilent 34401A, 6½ Digit Multimeter and using the previously determined average film thickness and surface area. Strain response was tested by applying a tensile strain using two different Instron-type strength testers and measuring resistance over a range of strains. Temperature response was tested by placing the test strips on a hotplate with a thermocouple used to measure temperature and taking resistance readings over a range of temperatures.

Once the basic sensor properties had been characterized and optimized sufficiently for the prototype array, array design and fabrication began. The initial

process used a series of etch steps to define the sensors and copper interconnects/leads. The process flow chart for this initial process is shown in Table I.

It was later determined that the etch steps presented too much possibility to damage the sensors and the process was altered such that sensor definition was accomplished via liftoff, and only the copper was patterned using an etch process. (The copper was able to be etched because its etch rate is so much faster than the Pt or NiCr that any damage to the Pt and NiCr sensors is negligible.) This second process is given in the flowchart in Table II.

Table I: Process Flowchart #1 for Array Prototype 1

Process Flow Chart - Sensory Array Model (1.0)

Process Step #	Individual Step #	Mask #	Material under processing	Process Description
1	1	--	Kapton	Cut and Clean Kapton - Use washes of Acetone, Methanol, or Isopropanol followed by Charlie's Soap® (Critical Cleaning Agent) and D.I. Water
2	2	--	Ti	Sputter blanket Ti adhesion layer (~100Å)
2	3	--	Pt	Sputter blanket Pt sensor layer (~2500Å)
3	4	--	Photoresist	Spin on photoresist
3	5	1	Photoresist	Mask and expose photoresist
3	6	--	Photoresist	Develop photoresist
4	7	--	Pt	Etch Pt sensors in hot aqua regia bath ($HCl+HNO_3$)
5	8	--	Photoresist	Remove remaining photoresist with acetone bath
6	9	--	NiCr	Sputter blanket NiCr sensor layer (~6000Å)
7	10	--	Photoresist	Spin on photoresist
7	11	2	Photoresist	Mask and expose photoresist
7	12	--	Photoresist	Develop photoresist
8	13	--	NiCr	Etch NiCr sensors in NiCr Etchant
9	14	--	Photoresist	Remove remaining photoresist with acetone bath
10	15	--	Cr	Sputter blanket Cr adhesion layer (~100Å)
10	16	--		Sputter blanket Cu conductor layer (~20000Å)
11	17	--	Photoresist	Spin on photoresist
11	18	3	Photoresist	Mask and expose photoresist
11	19	--	Photoresist	Develop photoresist
12	20	--	Cu	Etch Cu conductors in Cu Etchant
12	21	--	Cr	Etch in Cr etchant to clear remaining Cr
13	22	--	Photoresist	Remove remaining photoresist with acetone bath
14	23	--	Polyimide	Spin on polyimide insulator layer
15	24	4	Polyimide	Mask and expose polyimide insulator layer
15	25	--	Polyimide	Develop polyimide insulator layer and cure
16	26	--	Cr	Sputter blanket Cr adhesion layer (~100Å)
16	27	--	Cu	Sputter blanket Cu conductor layer (~20000Å)
17	28	--	Photoresist	Spin on photoresist
17	29	5	Photoresist	Mask and expose photoresist
17	30	--	Photoresist	Develop photoresist
18	31	--	Cu	Etch Cu conductors in Cu Etchant
18	32	--	Cr	Etch in Cr etchant to clear remaining Cr
19	33	--	Photoresist	Remove remaining photoresist with acetone bath
20	34	--	Final Insulator	Mask and spin on final insulator layer
21	35	--	Final Insulator	Develop final insulator layer and cure

Table II: Process Flowchart #2 for Array Prototype 1

Process Flow Chart - Sensory Array Model (Version 2.0)				
Process Step #	Individual Step #	Mask #	Material under processing	Process Description
1	1	N/A	Kapton	Cut and Clean Kapton - Use Charlie's Soap and DI water; **DO NOT** touch or wipe.
2	2	N/A	Photoresist	Spin on photoresist
2	3	1	Photoresist	Mask and expose photoresist
2	4	N/A	Photoresist	Develop photoresist
3	5	N/A	Ti	Sputter blanket Ti adhesion layer (~100Å)
3	6	N/A	Pt	Sputter blanket Pt sensor layer (~1700Å)
4	7	N/A	Pt	Liftoff photoresist with NMP bath to define Pt sensors
5	8	N/A	Photoresist	Rinse Kapton with Isopropyl and DI water
6	9	N/A	Photoresist	Spin on photoresist
6	10	2	Photoresist	Mask and expose photoresist
6	11	N/A	Photoresist	Develop photoresist
7	12	N/A	NiCr	Sputter blanket NiCr sensor layer (~3800Å)
8	13	N/A	NiCr	Liftoff photoresist with NMP bath to define Pt sensors
9	14	N/A	Photoresist	Rinse Kapton with Isopropyl and DI water
10	15	N/A	Cu	Sputter blanket Cu conductor layer (~10000Å)
11	16	N/A	Photoresist	Spin on photoresist
11	17	3	Photoresist	Mask and expose photoresist
11	18	N/A	Photoresist	Develop photoresist
12	19	N/A	Cu	Etch Cu condiutors in Cu Etchant
13	20	N/A	Photoresist	Remove remaining photoresist with acetone rinse
14	21	N/A	Polyimide	Spin on polyimide insulator layer
15	22	4	Polyimide	Mask and expose polyimide insulator layer
15	23	N/A	Polyimide	Develop and cure polyimide insulator layer
16	24	N/A	Cu	Sputter blanket Cu conductor layer (~10000Å)
17	25	N/A	Photoresist	Spin on photoresist
17	26	5	Photoresist	Mask and expose photoresist
17	27	N/A	Photoresist	Develop photoresist
18	28	N/A	Cu	Etch Cu condiutors in Cu Etchant
18	29	N/A	Cr	Etch in Cr etchant to clear remaining Cr
19	30	N/A	Photoresist	Remove remaining photoresist with acetone rinse
20	31	N/A	Final Insulator	Spin on final polyimide insulator layer
21	32	N/A	Final Insulator	Develop and cure final polyimide insulator layer

Please refer to the following illustrations (Figure 11a-e) for a very basic depiction of the processes used in the fabrication of the first prototype array.

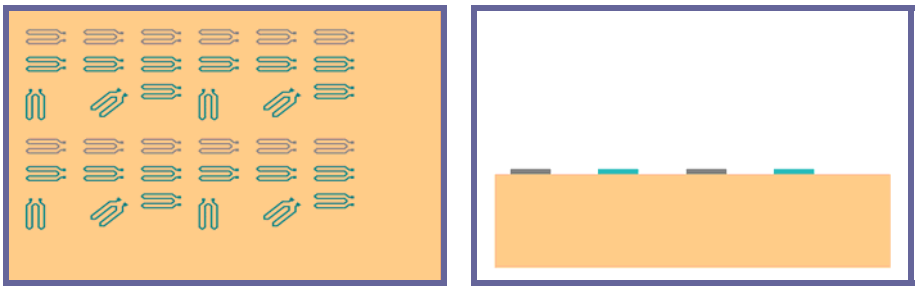

(a): Sensor Deposition and Definition

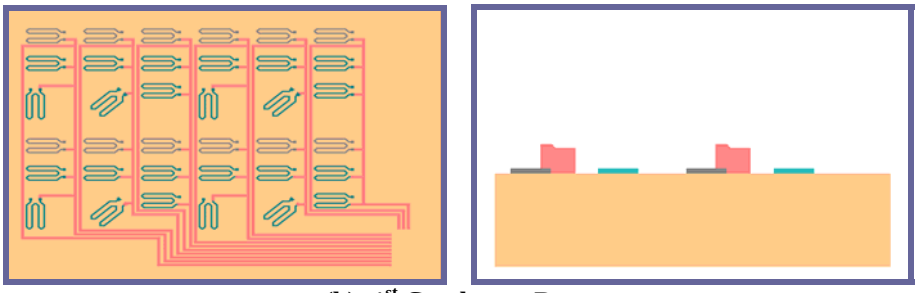

(b): 1st Conductor Runs

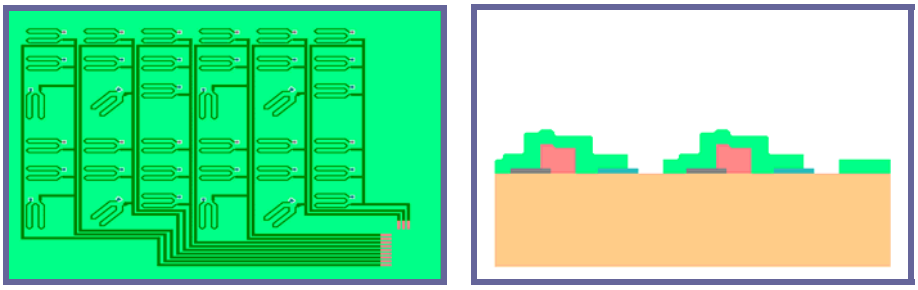

(c): Insulator and Vias

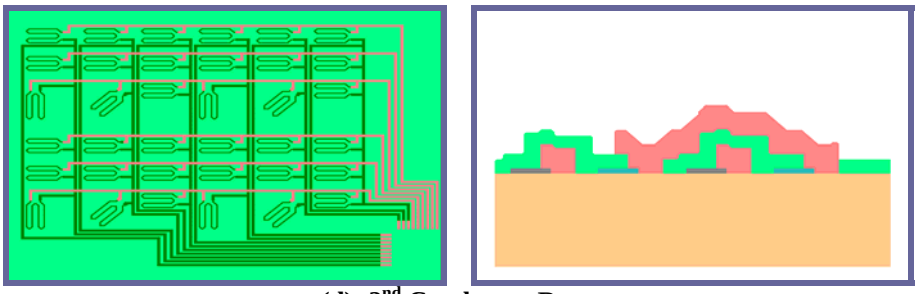

(d): 2nd Conductor Runs

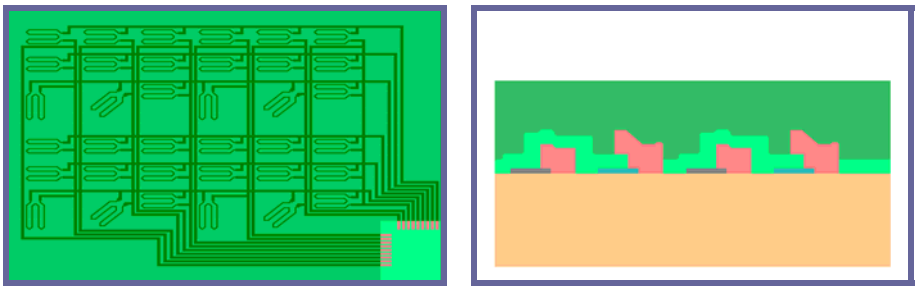

(e): Final Insulator Layer

Figure 11: Array 1 Fabrication Process Steps

Testing of the first prototype array was limited to verifying the temperature coefficient of resistance of the deposited sensors. This was accomplished by placing the array on a hot plate and raising temperature gradually over a predetermined range while monitoring and recording temperature and resistance. Resistance measurements were taken with an Agilent 34401A, 6½ Digit High-Precision Multimeter.

After the first prototype array was fabricated and tested, an error in the copper interconnect design pattern was discovered, requiring a complete redesign. The row/column address architecture is not feasible without switches or thin film transistors (TFTs) on the sensor array patch. The redesigned copper interconnects are based on a bank-switching approach, in which banks of sensors (each bank consisting of two strain rosettes, each with a temperature compensating Pt sensor) having one common line per bank, and individual 2nd lines to each sensor. By using the additional common line, we are essentially able to mimic a three-wire measurement for each sensor thus producing more accurate resistance measurements.

Because of the time involved in the redesign of the copper interconnects, we used the opportunity to redesign the sensor layout as well. During a meeting of QorTek, the Air Force and NCSU, the redesign was discussed and the agreed upon changes were as follows:

- Linear sensor dimensions ½ that of original array – occupying ¼ the original surface area
- Increased number of sensors on the same 6”x6” Kapton® patch
- Sensor-on-sensor design utilizing the photodefinable polyimide to allow a temperature sensor to be placed ~5μm directly above one of the strain sensors.

One key aspect of the new design (besides the Cirexx® prefabricated Cu lines for ease of connecting to control circuitry) is a set of contact resistance reference lines near the patch center connected to six in-line NiCr pads in electrical parallel and six in-line Pt pads in electrical parallel; the central space that these pads occupy may easily be used in the future for incorporating other desirable sensor types (acceleration, pressure, or air flow sensors).

Also, a new ribbon-connection from the sensor array to the sensor control chip was proposed and put into use to remove the sensor control chip from the sensor pad area. This was accomplished by having Cirexx® prefabricate the polyimide patches with a connecting "tail" design (instead of the previously used square Kapton® sheets). The process chart for this redesigned prototype array is given in Table III.

Table III: Prototype Array 2 Process Flowchart

Process Flow Chart - Sensory Array Model (Version 3.0)				
Process Step #	**Individual Step #**	**Mask #**	**Material under processing**	**Process Description**
1	1	----------	Kapton	Clean Cirexx Patch: Rinse with Acetone, Methanol & Isopropanol. Then use Charlie's Soap® (critical cleaning soap) and DI water, **DO NOT** touch/wipe - blow dry w/compressed air.
2	2	----------	Cirexx Copper	Partially etch Cirexx Copper pads to thin them
3	3	----------	Kapton	Clean Kapton with Charlie's Soap® (critical cleaning soap) and DI water, **DO NOT** touch/wipe - blow dry w/compressed air.
3	4	----------	Kapton	Evaporate water from patch by placing on 110ºC hot plate for approximately 10 minutes
4	5	----------	Polyimide	Spin on polyimide insulator layer
4	6	SM	Polyimide	Shadowmask and expose polyimide insulator layer
4	7	----------	Polyimide	Develop polyimide insulator layer
4	8	----------	Polyimide	Cure polyimide insulator layer
5	9	----------	Kapton	Clean Kapton as described in individual step #3
6	10	----------	Photoresist	Spin on photoresist
6	11	1	Photoresist	Mask and expose photoresist
6	12	----------	Photoresist	Develop photoresist
7	13	----------	Ti	Shadowmask & Sputter blanket Ti adhesion layer (~100Å)
7	14	----------	Pt	Shadowmask & Sputter blanket Pt sensor layer (~1700Å)
8	15	----------	Pt	Liftoff photoresist with NMP bath to define Pt sensors
9	16	----------	Photoresist	Clean Kapton as described in individual step #1
10	17	----------	Polyimide	Spin on polyimide insulator layer
10	18	2	Polyimide	Mask and expose polyimide insulator layer
10	19	----------	Polyimide	Develop polyimide insulator layer
10	20	----------	Polyimide	Cure polyimide insulator layer
11	21		Kapton	Clean Kapton as described in individual step #3
12	22	----------	Photoresist	Spin on photoresist
12	23	3	Photoresist	Mask and expose photoresist
12	24	----------	Photoresist	Develop photoresist
13	25	----------	NiCr	Shadowmask & Sputter blanket NiCr sensor layer (~3800Å)
14	26	----------	NiCr	Liftoff photoresist with NMP bath to define NiCr sensors
15	27	----------	Kapton	Clean Kapton as described in individual step #1
16	28	----------	NiCr	Shadowmask & Sputter blanket NiCr adhesion layer (~100Å)
16	29	----------	Cu	Shadowmask & Sputter blanket Cu conductor layer (~10000Å)
17	30	----------	Photoresist	Spin on photoresist
17	31	4	Photoresist	Mask and expose photoresist
17	32	----------	Photoresist	Develop photoresist
18	33	----------	Cu	Etch Cu conductors in Cu Etchant
18	34	----------	Photoresist	Remove remaining photoresist with acetone rinse
19	35	----------	Kapton	Clean Kapton as described in individual step #1
20	36	----------	Final Insulator	Spin on final polyimide insulator layer
20	37	----------	Final Insulator	Cure final polyimide insulator layer

The second prototype array was tested for both strain and temperature response. Temperature response was accomplished by the same procedure documented for the first prototype array. Strain response was accomplished by attaching two pieces of aluminum bar-stock to the top and two to the bottom of the array (to minimize stress concentration and prevent tearing of the array) and then subjecting the array to a range of controlled strain steps using an Instron-type strength tester. The strain and resistance of sensors was recorded throughout the full range of applied strain.

The third and final prototype array was created as a demonstration of scalability of the overall design. A duplicate of the second prototype array was created with sensors of the same overall thickness, and the same intended target resistance, but half the length and width of the second array sensors. This array occupied an area of ~ 1" x 1" square and was patterned to fit the Cirexx® contact pads on the same prefabricated polyimide patches as the second array. This prototype array was patterned using the same flowchart as the second array, with one additional step. Following step 32 from Table III, the copper photoresist pattern was completed by hand to connect the Cirexx® patch copper pads to the array leads.

The scalability of the array design is further illustrated in the following equations. $R = \rho\left(\frac{length}{(film\ thickness \times width)}\right)$ This describes resistance (R) as a function of resistivity (ρ) and film length, width and thickness. For example, in the NiCr sensor design the film length was 2.8×10^{-2}m, the width was 4.4×10^{-4}m and the thickness was 7×10^{-7}m. In the next two equations it can be show that by using the same material with the same

thickness, and scaling the length and width by ½ their original values, the sensor will be maintained at 100Ω of resistance.

- Initial resistor: $100\Omega = 1.10\times10^{-6}\,\Omega m\left(\frac{2.8\times10^{-2}\,m}{7.0\times10^{-7}\,m\times4.4\times10^{-4}\,m}\right)$
- Scaled by ½ : $100\Omega = 1.10\times10^{-6}\,\Omega m\left(\frac{1.4\times10^{-2}\,m}{7.0\times10^{-7}\,m\times2.2\times10^{-4}\,m}\right)$

FINAL PROCESS DESCRIPTION

The following is a detailed description of the final process developed for the fabrication of the second prototype sensor array and outlined in Table III above.

Step 1: Clean the Cirexx® patch. Begin with an acetone wash followed by subsequent washes in methanol and isopropanol. After the isopropanol rinse, the Cirexx® patch is blown dry using compressed nitrogen. When the patch is dry, spray patch with Charlie's Soap® (A critical cleaning surfactant) and rinse thoroughly with DI Water. Blow patch dry with compressed nitrogen.

Step 2: Place the Cirexx® patch in a plastic tray and deposit a "bead" of FeCl copper etchant around the pre-fabricated copper contact pads. Ensure the etchant only contacts the pads on the *interior* portion of the patch, and that on about ½ of the contact pad is covered with etchant. Allow the etchant to rest for 25 minutes. Rinse the patch with DI water, then immerse in a bath of dilute Ammonium Persulfate Cu etchant to clean any oxidized Cu. Rinse in DI Water. (This etch process is needed to thin the step height at the edge of the Cirexx® Cu so that the sputter-deposited Cu will make a complete electrical connection)

Step 3: Spray patch with Charlie's Soap® and rinse thoroughly with DI Water. Blow patch dry with compressed nitrogen.

Step 4: Immediately prior to the polyimide application in step 5, place the patch onto a hotplate at 110ºC and allow ~10 minutes for water to evaporate from the surface.

Step 5: Spin HD-4000 photodefinable polyimide onto the patch

Step 6: Using a shadow mask, expose the HD-4000 using a Karl Suss MA-6 or similar photolithographic aligning tool. Based on exposure system light intensity, calculate exposure duration recommended by manufacturer and expose the patch in area that reaches from the outside patch edge to the inner 75% of the copper contact pads (89mm x 89mm). Soft Bake the HD-4000 for ~5 minutes @ ~100ºC.

Step 7: Develop the polyimide using three-step bath process. Baths are as follows: 100% developer bath ~45 seconds, 50% developer/50% rinse bath ~45 seconds, 100% rinse bath ~45 seconds, using the chemicals supplied by the manufacturer. Rinse the patch with DI water and blow dry with compressed nitrogen.

Step 8: Place the patch into a furnace containing a flow of hydrogen forming gas and cure the polyimide square to ~325ºC for one hour, leaving a smooth square of fresh polyimide in the center of the patch. Use the following schedule: Ramp up temperature to 325ºC at 10ºC/minute; dwell for 1 hour; ramp down to 50ºC at 20ºC/minute.

Step 9: When the furnace has cooled to within 50ºC of ambient, remove the patch and clean as described in step 3.

Step 10: Spin JSR NFR016D Series negative photoresist onto the patch. Soft bake the photoresist.

Step 11: Using the Pt sensor mask (mask #1), expose the negative photoresist using A Karl Suss MA-6 or similar aligning tool. Based on exposure system light intensity, calculate exposure duration recommended by manufacturer and expose photoresist. Post Expose-Bake the photoresist.

Step 12: Develop the photoresist for 45-60 seconds in MF-319 developer solution, rinse with DI water bath for ~60 seconds and blow dry with compressed nitrogen.

Step 13: Load the NiCr or Cr target into the DC magnetron. Place the square shadow mask onto the Cirexx® patch and sputter ~100Å of adhesion metal onto the patch.

Step 14: Load the Pt target into the DC magnetron. Affix the patch (using cellophane tape) to an aluminum heat sink of the same area as the patch and ¼" thick. Place the square shadow mask onto the Cirexx® patch and sputter ~1700Å of Pt onto the patch. Minimize continuous sputter duration (15-20 seconds per burst with ~40 seconds wait between bursts) to minimize excessive heat-hardening of the photoresist.

Step 15: Remove the patch from the magnetron and place in a bath of N-Methyl Pyrrolidone (NMP) which has been heated to ~65ºC and ***GENTLY*** flush until Pt liftoff is complete and Pt sensors are defined (10-45 minutes).

Step 16: Clean Cirexx® patch as described in Step 1.

Step 17: Spin HD-4000 photodefinable polyimide onto the patch. Soft Bake the HD-4000.

Step 18: Using the polyimide insulator mask (mask #2) expose the HD-4000 using A Karl Suss MA-6 or similar aligning tool. Based on exposure system light intensity, calculate exposure duration recommended by manufacturer and expose the HD-4000. Soft Bake the HD-4000.

Step 19: Develop the polyimide using three-step bath process. Baths are as follows: 100% developer bath ~45 seconds, 50% developer/50% rinse bath ~45 seconds, 100% rinse bath ~45 seconds, using the chemicals supplied by the manufacturer. Rinse the patch with DI water and blow dry with compressed nitrogen.

Step 20: Place the patch into a furnace containing a flow of hydrogen forming gas and cure the polyimide square to ~325ºC for one hour. Use the following schedule: Ramp up temperature to 325ºC at 10ºC/minute; dwell for 1 hour; ramp down to 50ºC at 20ºC/minute.

Step 21: When the furnace has cooled to within 50ºC of ambient, remove the patch and clean as described in step 3.

Step 22: Spin JSR NFR016D Series negative photoresist onto the patch. Soft bake the photoresist.

Step 23: Using the NiCr sensor mask (mask #3), expose the negative photoresist using A Karl Suss MA-6 or similar aligning tool. Based on exposure system light intensity, calculate exposure duration recommended by manufacturer and expose photoresist. Post Expose-Bake the photoresist.

Step 24: Develop the photoresist for 45-60 seconds in MF-319 developer solution, rinse with DI water bath for ~60 seconds and blow dry with compressed nitrogen.

Step 25: Load the NiCr target into the DC magnetron. Affix the patch (using cellophane tape) to an Aluminum heat sink of the same area as the patch and ¼" thick. Place the square shadow mask onto the Cirexx® patch and sputter ~3800Å of Pt onto the patch. Minimize continuous sputter duration (15-20 seconds per burst) to minimize excessive heat-hardening of the photoresist.

Step 26: Remove the patch from the magnetron and place in a bath of N-Methyl Pyrrolidone (NMP) which has been heated to ~65ºC and *GENTLY* flush until Pt liftoff is complete and Pt sensors are defined. 10-45 minutes.

Step 27: Clean Cirexx ® patch as described in Step 1.

Step 28: Load the NiCr or Cr target into the DC magnetron. Place the square shadow mask onto the Cirexx® patch and sputter ~100Å of adhesion metal onto the patch.

Step 29: Load the Cu target into the DC magnetron. Affix the patch (using cellophane tape) to an Aluminum heat sink of the same area as the patch and ¼" thick. Place the square shadow mask onto the Cirexx® patch and sputter ~10000Å of Pt onto the patch. Minimize continuous sputter duration (15-20 seconds per burst) to minimize excessive heat-hardening of the photoresist.

Step 30: Spin Shipley 1813 series photoresist onto the patch. Soft bake the photoresist.

Step 31: Using the Cu Interconnect mask (mask #3), expose the Shipley 1813 photoresist using A Karl Suss MA-6 or similar aligning tool. Based on exposure system light intensity, calculate exposure duration recommended by manufacturer and expose photoresist.

Step 32: Develop the photoresist for 45-60 seconds in MF-319 developer solution, rinse with DI water bath for ~60 seconds and blow dry with compressed nitrogen.

Step 33: Etch Cu interconnects in Ammonium Persufate etchant until Cu interconnects are defined (5-10 minutes).

Step 34: Remove the remaining photoresist with an acetone rinse

Step 35: Clean Cirexx ® patch as described in Step 1.

Step 36: Spin Pyralin PI 2525 polyimide onto the patch. Soft Bake the Pyralin PI 2525.

Step 37: Place the patch into a furnace containing a flow of hydrogen forming gas and cure the polyimide square to ~325ºC for one hour. Use the following schedule: Ramp up temperature to 325ºC at 10ºC/minute; dwell for 1 hour; ramp down to 50ºC at 20ºC/minute. Remove and store patch for delivery.

MATERIALS USED

DuPont Kapton® – substrate for initial design and testing

Cirexx® Prefabricated Patch – substrate for second generation array design

- DuPont Pyralux® AP Laminate (Tested – Not Used in Final Prototype)
- DuPont Pyralux® LF Sheet Adhesive (Tested – Not Used in Final Prototype)
- DuPont Pyralux® FR Coverlay (Tested – Not Used in Final Prototype)
- DuPont Pyralux® FR Cu-Clad Laminate

Hitachi HD 4000

Hitachi PA 400D Developer & PA 400R Rinse

Pyralin PI 2525

JSR Electronics NFR016

Shipley 1813 Photoresist

MF-319 Developer

N-Methyl Pyrolidinone

Ammonium Persulfate (Cu Etchant)

Ferric Chloride (Cu Etchant)

Sutherland Products Charlie's Soap®

Photomasks (Photo Sciences)

RESULTS AND DISCUSSION

INITIAL RESEARCH GOAL SUMMARY

1) Fabricate basic sensor elements on Kapton®

2) Test sensor element materials after sputtering for:

   a) Characteristic electrical response to strain variance

   b) Characteristic electrical response to temperature variance

   c) Mechanical stability and adhesion to Kapton®

3) Design array layout and begin fabrication of prototype array

Year-1 demonstration goals required sufficient sensor thickness uniformity over the array area to create sensors of reasonably similar resistance values. To that end, Pt films were deposited and examined to determine film uniformity and film properties under different deposition conditions. For a DC magnetron such as the one used in this project, the two conditions primarily known to affect thin film uniformity are substrate-target distance, and chamber pressure. Figure 12 shows the results of the initial studies of the effects of thickness vs. distance from the center of the target. Film thickness (in Angstroms) was measured using a Sloan Dektak II profilometer.

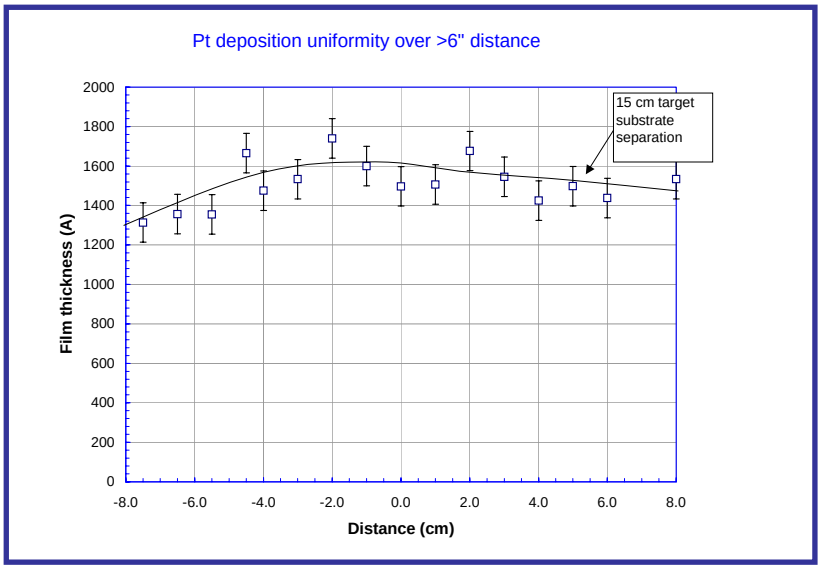

Figure 12: Pt Deposition Uniformity Over >6" Length vs. Distance from Target Center

Initial film thickness uniformity data is shown below in Table IV. Measurements were taken using a Dektak profilometer. Measurements represent approximately a 4"×4" deposition area. Based on the data from Table IV, film thickness uniformity was acceptable for initial testing and prototype development. However, the deposition process will require further refinement before development of a production-scale process. Initial test results indicate that higher-tolerance film uniformity will be possible via alteration of deposition conditions and/or deposition technique. The ±10% level of film uniformity achieved could be further improved by optimizing process conditions, and using photo-lithographically defined edge steps for better measurement precision.

Initial studies of Pt film resistivity indicate a resistivity value (35 μΩ-cm deposited on glass) much higher than the bulk value of 10.7 μΩ-cm at room temperature. Higher values of resistivity are common for thin films due to impurities and/or film stress; upon later examination, the resistivity of the film seems to be a good predictor of

overall sensor performance, with higher resistivity values corresponding to smaller overall grain sizes in the film and relatively poor sensor performance, (particularly in strain-response testing).

From the data in Table V, NiChrome as-deposited average resistivity values deviate from literature values by a factor of approximately seven. This also requires further optimization, which will be achieved by modifying deposition conditions. Platinum as-deposited average resistivity values deviate by a factor of ~3 from literature values. This is generally regarded as acceptable for sputter deposition of metals.

Table IV: Average Thickness Data for NiCr Films

Average Thickness Data for NiCr Film			
Both films deposited under the following conditions:			
Background Pressure = 1.4E-5 Torr			
Magnetron Power = 250W			
Target Height = 15cm			
Sample: 6/14/04 :001		Sample: 6/14/04 :002	
Ar Press: 6mTorr		Ar Press: 15mTorr	
	3707		3683
	3905		3675
	3695		3812
	3815		3877
	4000		4142
	4040		3811
	4006		3650
	3890		3635
	3840		4108
	3650		
	3427		
	3935		
	3844		
Mean	3827.231	Mean	3821.444
StDv	171.4668	StDv	191.3512

Individual test resistors were fabricated and film resistivity was calculated based on average film thickness values and measured resistances. The results of resistivity calculations for five (5) NiChrome and two (2) Platinum strips are recorded in Table V.

Table V: Pt & NiCr Film Resistivities

Literature	Substrate	Sample	Calculated Resistivities			
NiChrome	Glass	001	3.79E-06	3.93E-06	4.15E-06	4.43E-06
1.10E-06		002	1.27E-06	1.18E-06	1.2E-06	1.24E-06
	Kapton	1	6.83E-06	3.49E-06	3.63E-06	4.43E-06
		2	4.06E-06	3.61E-06	3.52E-06	3.06E-07
		3	4.21E-06	7.73E-05	1.26E-05	7.13E-06
Platinum	Kapton	1	3.52E-07	3.11E-07	3.05E-07	3.02E-07
1.06E-07		2	4.08E-07	3.66E-07	3.62E-07	3.82E-07

Resistance was measured with respect to strain for Platinum and NiChrome samples on two different strength testing machines, and the results of those measurements are detailed in Figures 13-16. NiChrome resistance with strain is shown in Figures 13 and 15. Problems with the testing apparatus, e.g. sample slippage, caused the Figure 13 data to be incorrect. Figure 15 shows a trend line estimating projected elastic response of the as-deposited sample. In Figures 14 and 16, platinum resistance change with strain is shown. Response appears to be elastic and data trends are repeatable. The as-deposited film does not show an ideal strain response, most likely due to residual compressive stress. However, this does not alter reliability or repeatability of the material's response to strain; only the magnitude of the strain response is affected.

In Figure 15 NiChrome sample D-5, the linear regression only considers the first 7 (pink) data points, since the other points are believed to represent plastic strain. Also, the data points are generally very scattered and do not represent ideal linear elastic strain response. One possible reason for this is the technique used to hold the test strips in the strength tester. Due to the available chucks for the instruments, a sufficiently bulky and

robust surface needed to be created for the chuck to bite into. After testing several possible materials a Devcon® epoxy (Plastic Welder™) was determined to be the best solution. The Plastic Welder™ bonded sufficiently to the Kapton® to allow the strength test and allowed the chuck to grip as well; however, the elastomeric properties of the Kapton® were a problem as strain relaxation occurred during testing. The Kapton® was tested without being adhered to a more rigid body, as would be the situation in actual operation. Without the benefit of a more rigid, uniformly strained material, the strains experienced by the films on the Kapton® would be non uniform and would indicate any localized high-strain, not the average strain. In the future, automated data collection should be employed to minimize the time required to take measurements to a negligible value, thus allowing very little time for any strain relaxation effects to skew the data. In addition, the Kapton® patch should be adhered to another surface, e.g. a sheet of aluminum, or some other material with a more uniform strain response. Also – adhesion problems between the deposited films and the Kapton® may have contributed to the poor strain response data.

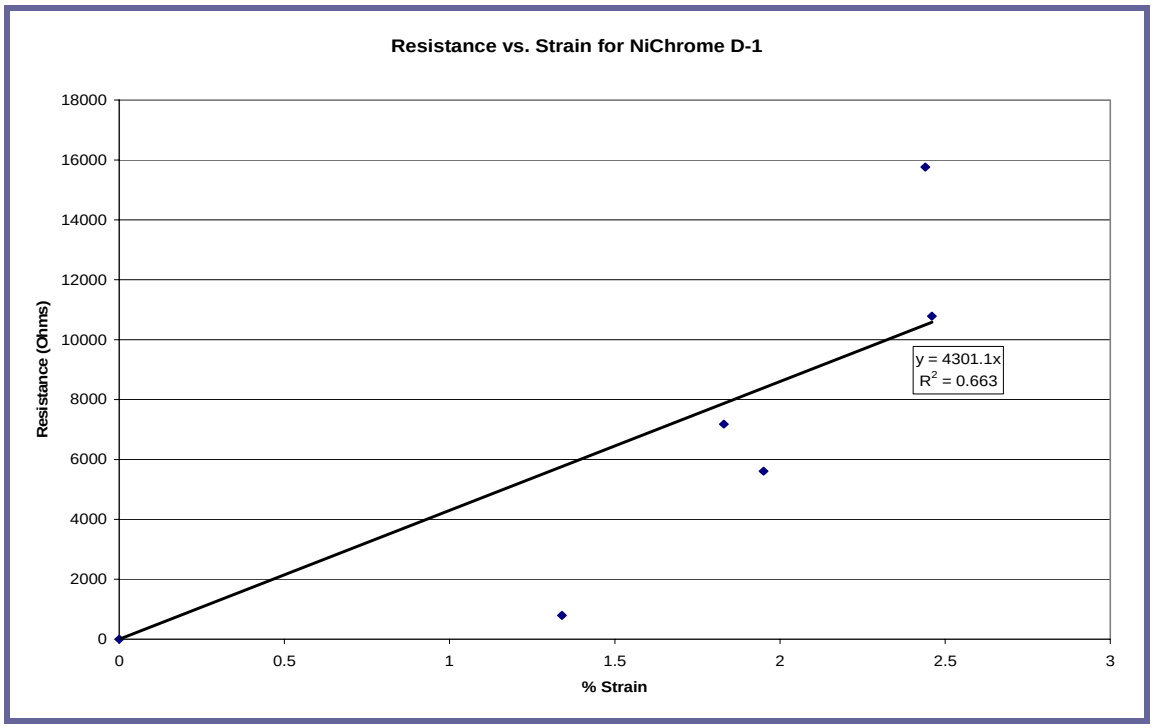

Figure 13: Resistance vs. Strain for NiChrome Test Strip D-1

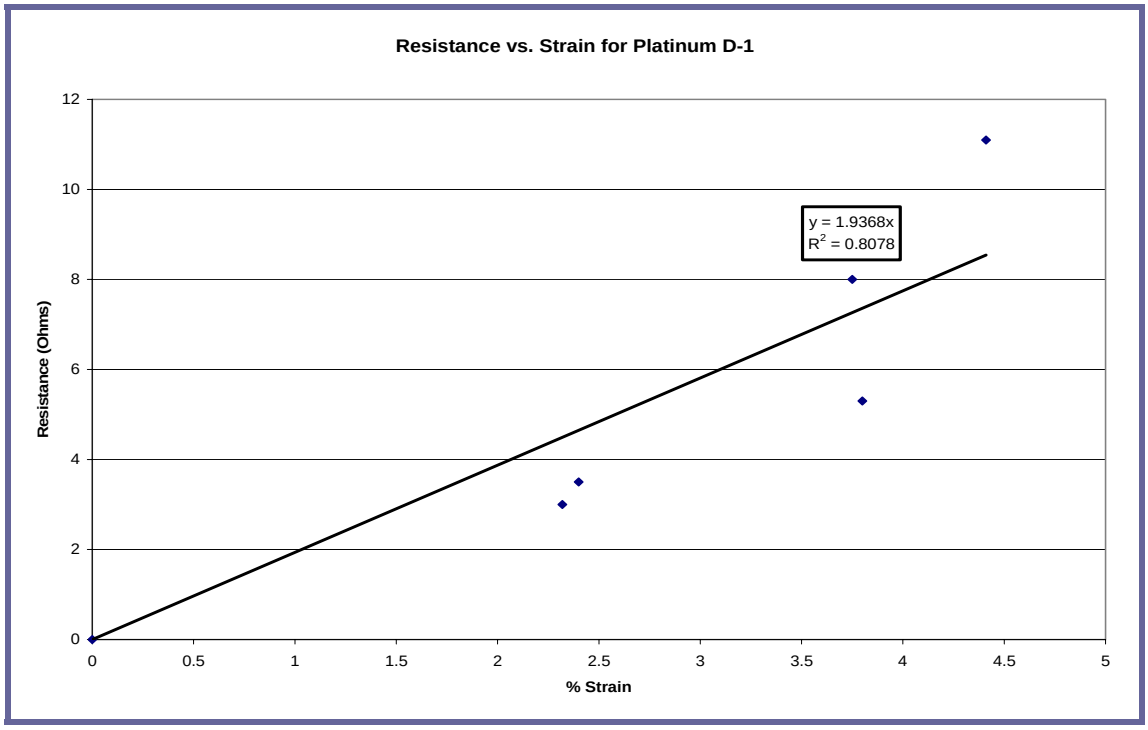

Figure 14: Resistance vs. Strain for Platinum Test Strip D-1

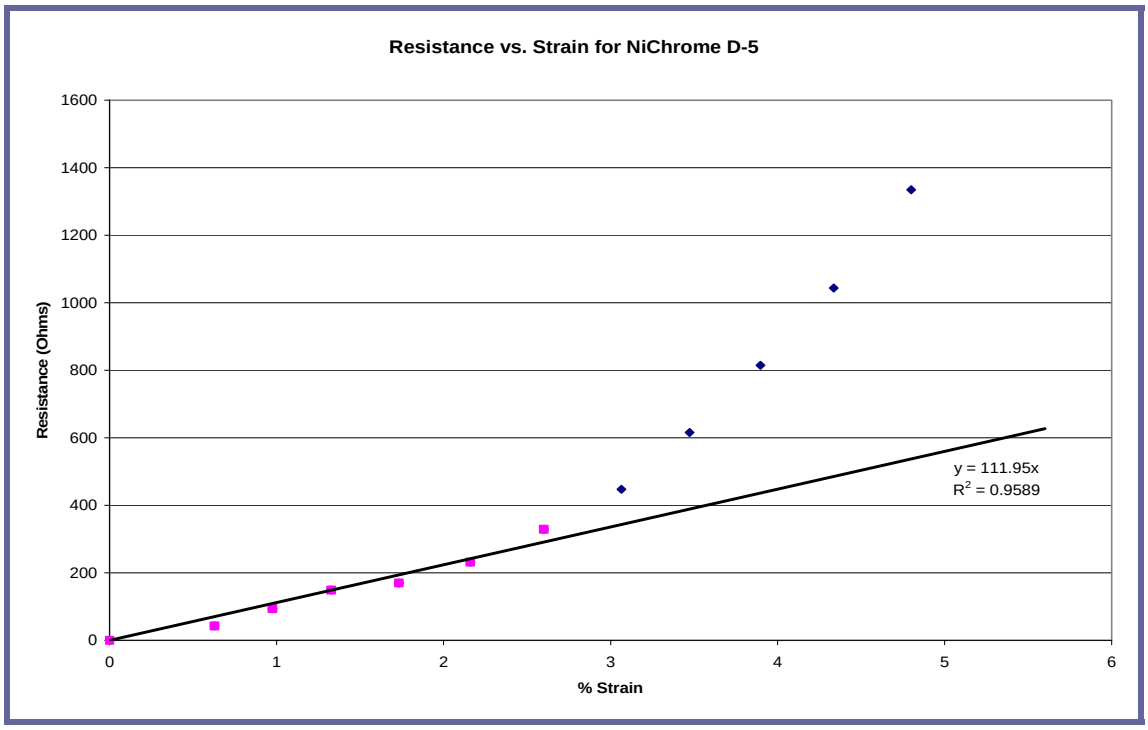

Figure 15: Resistance vs. Strain for NiChrome Test Strip D-5

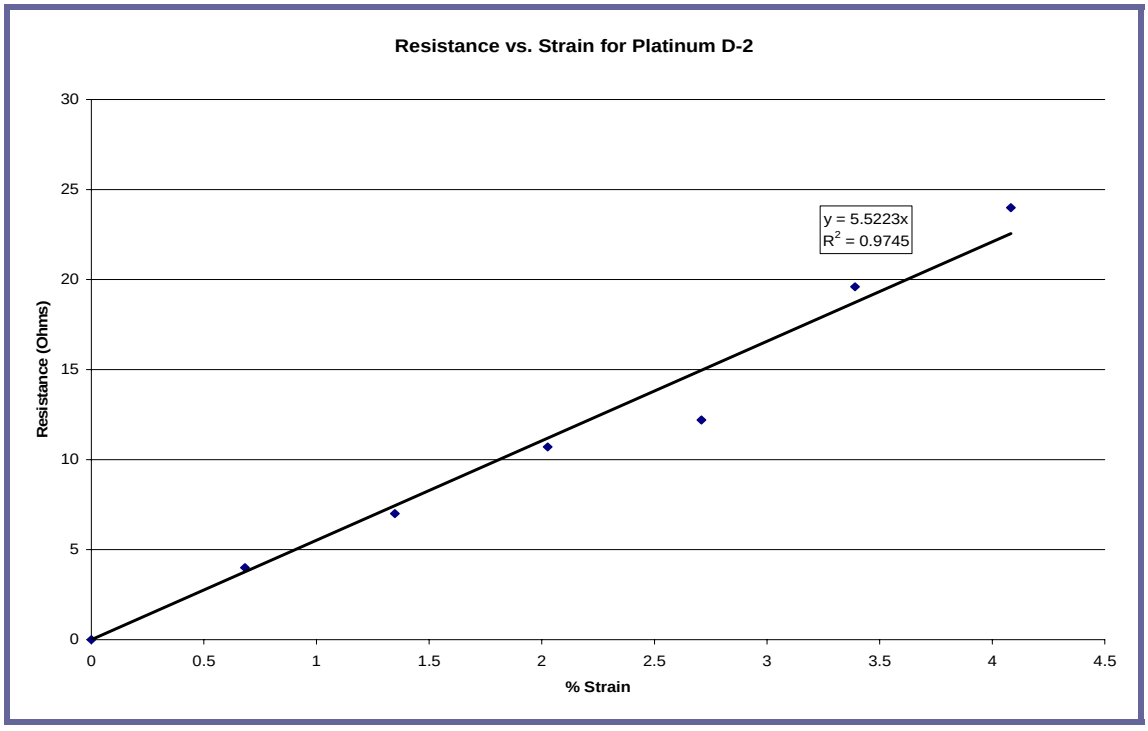

Figure 16: Resistance vs. Strain for Platinum Test Strip D-2

X-Ray diffraction on the deposited NiCr films produced a pattern consistent with amorphous materials, which indicates very small grain size. Purely qualitative analysis of the diffraction pattern shown in Figure 17 indicates a NiCr grain size of ~10nm. Also in Figure 17, the crystalline structure of the Kapton® substrate is clearly visible and is of sufficient intensity that the NiCr peak is essentially undetectable. A Pt XRD graph is shown in Figure 18, and has clearly well-defined peaks.

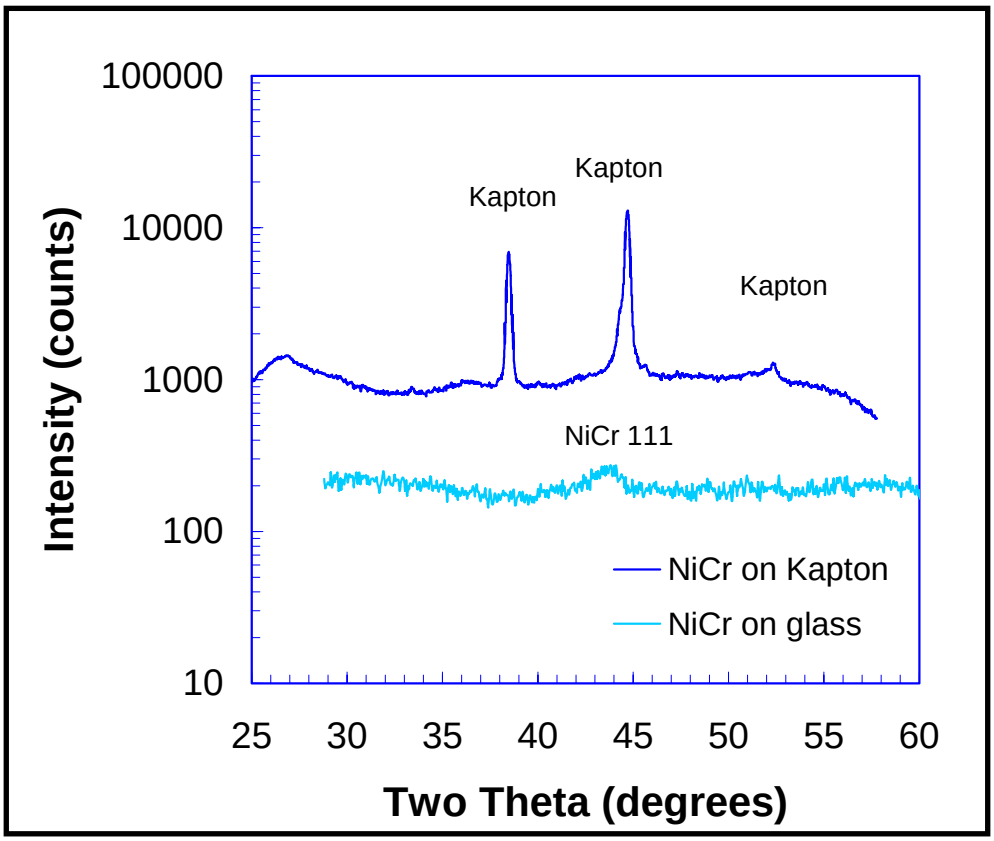

Figure 17: XRD Data of Sputtered NiCr Films on Kapton and Glass

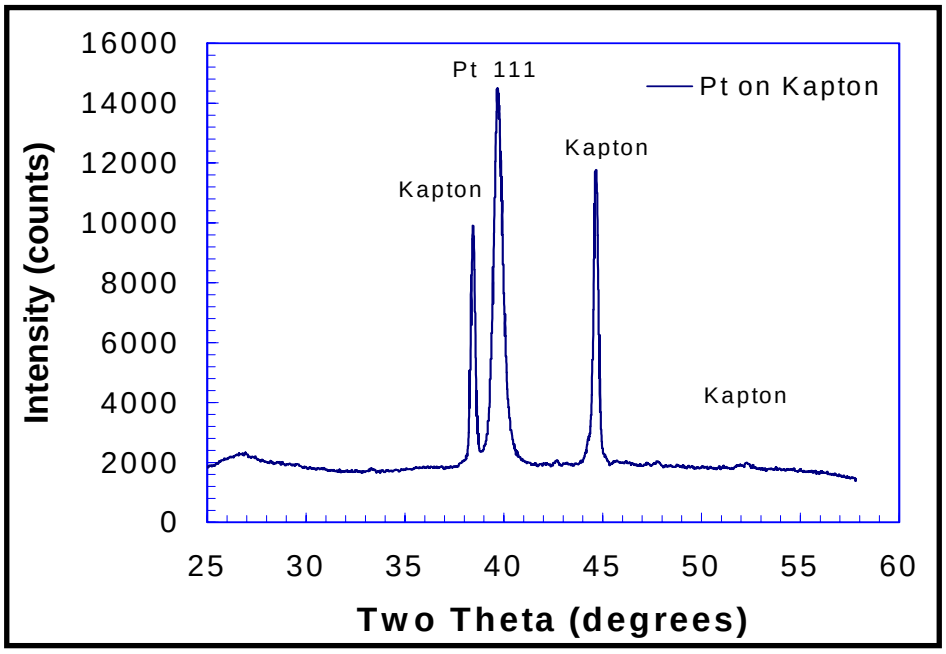

Figure 18: XRD Data of Sputtered Pt Film on Kapton

One probable reason for the very small grain size of the deposited NiCr related to oxygen impurities. NiCr is reactive with oxygen, which results in pinning of grain boundaries which in turn limits diffusion at the grain boundaries and thus limits grain growth. Research by T. M. Nenadovic indicates that not only are sputtered NiCr films susceptible to oxygen related interference of grain growth, but that if the target composition is 20% Cr, the sputtered film composition may be as high as 45%Cr[10]. Reed-Hill suggests that in a binary alloy, that lattice strain energies due to impurity atoms may inhibit grain growth as might the addition of impurities such as oxygen, even in minute quantities[11]. From the remaining data in this figure, it is clear that the material's response is not purely elastic, but rather shows the effects of extremely small grain size combined with potential oxygen impurities. The Hall-Petch relation also suggests that as grain size decreases, ductility does as well. It is believed that higher system thermal

energy during deposition will allow larger grains to grow, and also will help to relieve residual tensile stress in the as-deposited film.

Measurements of resistance vs. temperature were taken on a Platinum test strip and a NiChrome test strip; the results are graphed in Figures 19 and 20. In Figure 19, NiChrome sample C-2, the linear regression only considers the first 6 (pink) data points. It was apparent that after this point the data was no longer responding in a linear fashion and the resistance with temperature response reflects similar behavior to the resistance with strain response. The small grain size, possible oxygen impurities and residual tensile stress in the NiCr films mentioned previously is believed to be the primary factor responsible for this behavior. Platinum resistance with temperature, shown in Figure 20, is nearly perfectly linear, but again is not consistent in magnitude with literature values due to residual compressive stresses in the material.

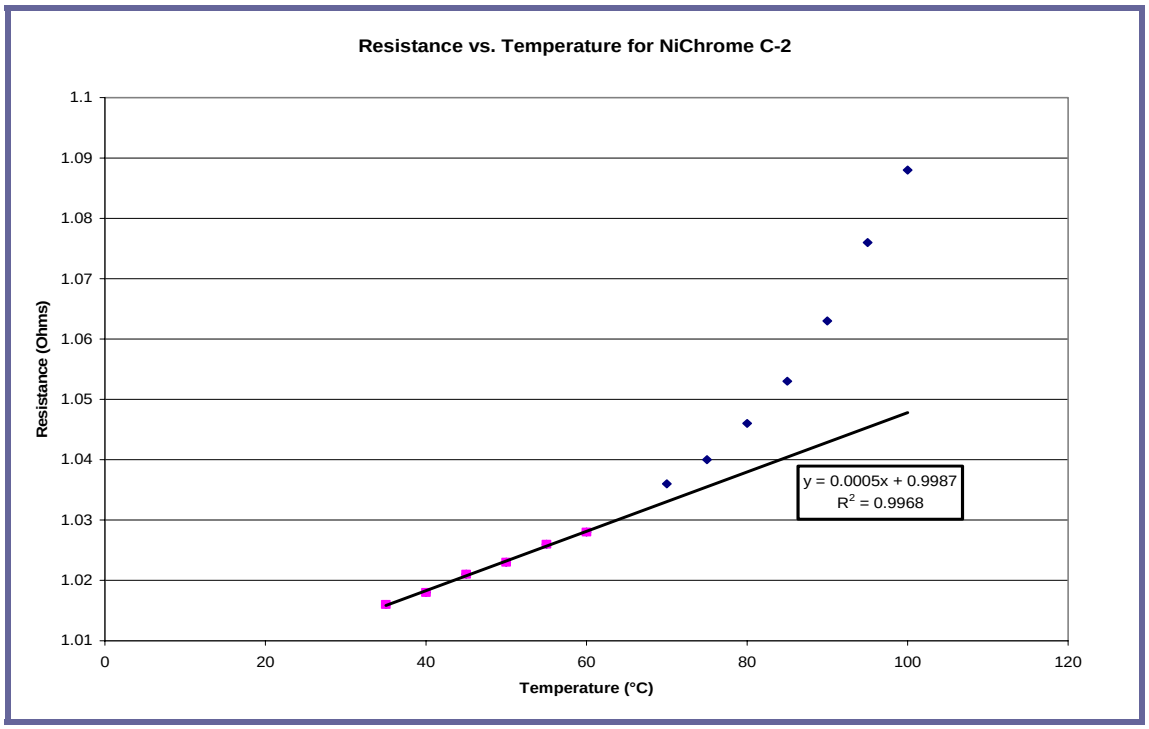

Figure 19: Resistance vs. Temperature for NiCr Test Strip C-2

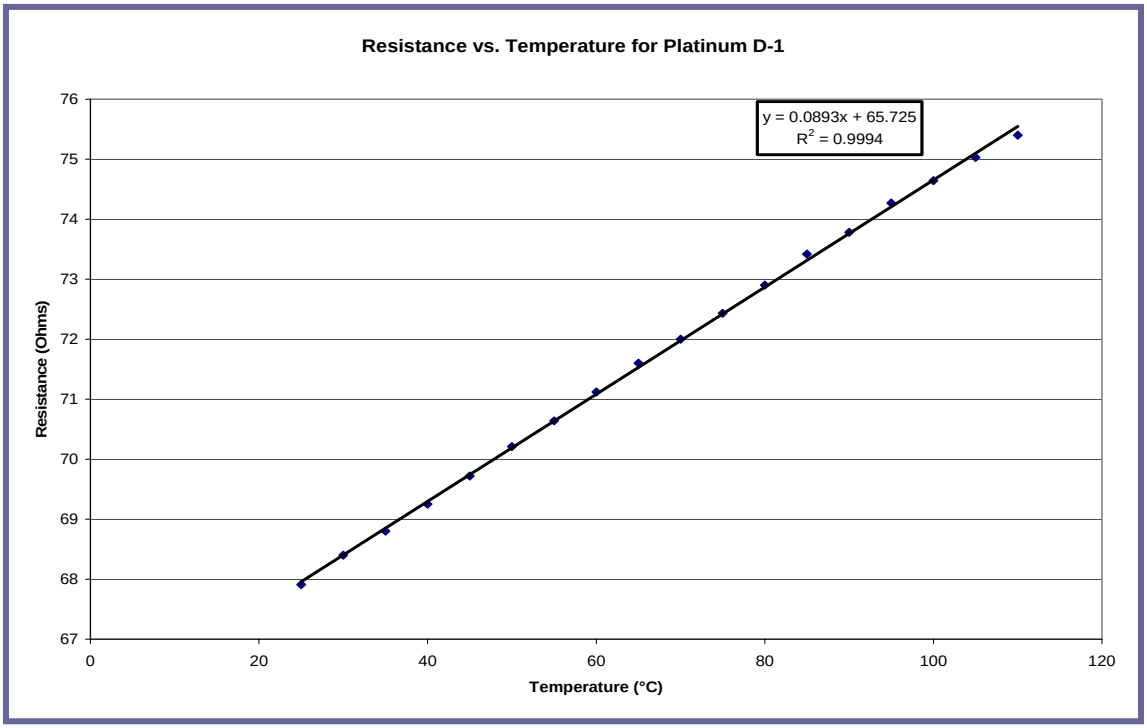

Figure 20: Resistance vs. Temperature for Pt Test Strip D-1

Table VI is a properties summary of the current as-deposited films. Values are listed and compared to literature values for TCR, Strain Sensitivity and Resistivity.

Table VI: Materials Properties Summary of Sputtered Films

Materials Properties		
	Literature Values	Current as-deposited values
Platinum		
TCR/°C	3.93E-03	2.18E-03
Strain Sensitivity	6.10E+00	4.45E+00
Resistivity(Ωm)	1.06E-07	3.49E-07
NiChrome		
TCR/°C	2.00E-04	3.00E-04
Strain Sensitivity	2.10E+00	1.80E+00
Resistivity(Ωm)	1.10E-06	7.62E-06

ADHESION ISSUES

In order to achieve adhesion of the Pt film to Kapton® or other polyimide films a thin ~100Å layer of Ti (later NiCr) was sputtered prior to the Pt. This type of procedure should be carried out with a two-magnetron system, to avoid exposing the adhesion metal to air. We were unable to do this because our DC system only has a single magnetron – we therefore simply minimized the time that the adhesion layer was exposed to air. In order to achieve adhesion of the Cu film to Kapton® or other polyimide films a thin ~100Å layer of Cr or NiCr was sputtered prior to the Cu. Tests were carried out to determine if the Cu required and adhesion metal layer and the results were inconclusive. In some instances the Cu seemed to adhere very well without the layer and in others it peeled off during the etch process. It was decided to use the adhesion layer for the duration of this project.

LARGE-AREA SCALING ISSUES

The typical target-to-substrate height used in our sputtering system is ~5cm and is generally intended to uniformly deposit onto a circular area of about 3-4" in diameter. In order to achieve the best possible uniformity over a 5-5½" radius area, using the equipment we have, the target-to-substrate height must be increased. By varying power, pressure and target-substrate distance in the magnetron, one essentially varies the rate of material deposition, the amount of heating the substrate receives, the energy with which the deposited material bombards the substrate and the concentration distribution of the deposited material as it bombards the substrate. All of these changes affect the overall quality of the deposited films and do not guarantee a uniform film thickness. A

significant improvement would be achieved with a rotating substrate holder, but again, that particular process refinement was unavailable to us at the time of this research.

RESIDUAL STRESS ISSUES

Another problem encountered in the processing of the array prototypes was the occurrence of residual stress as an artifact of the DC magnetron sputtering. Because the Kapton® used in the prototype array was only 75μm thick, the effect of residual stresses in the deposited films could be directly observed by cutting a small strip of Kapton® (e.g. 1"x3") and sputtering 500-1000Å of metal onto the surface. The stress effects are categorized in Figure 21a-c. Figure 21a indicates a film with a compressive stress which causes the Kapton® to curl slightly upward, 21b shows an essentially neutral stress while 21c shows the slight downward curl associated with a tensile stress. The effects of excessive tensile or compressive stresses can lead to cracking and delamination, respectively, of the deposited sensor during patterning. These stresses result from deposition conditions within the magnetron. As magnetron power, target to substrate distance and pressures are varied, the energy with which the deposited specie impacts the target is likewise varied. Target to substrate distance combined with pressure are the primary factors involved in film thickness uniformity, and once optimized leave essentially magnetron power as the primary factor to compensate for residual stresses. Figure 22 illustrates what happens to a NiCr strain gage after processing when deposition occurred under excessive compressive stress.

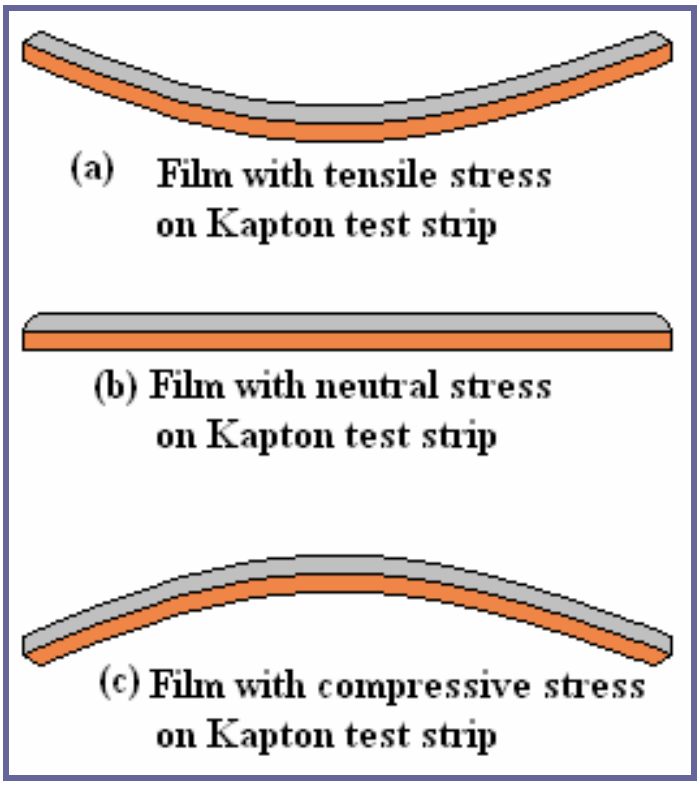

Figure 21: Novel Technique for Determination of Residual Stress in Sputtered Films

Figure 22: NiCr Sensor Peeling/Wrinkling Due to Excess Compressive Stress

Another problem that needed to be dealt with was the presence of surface artifacts on the Kapton® and later on the Cirexx® patches. Figure 23 illustrates the result of a very light scratch in the surface of a piece of Kapton®. The large diagonal scratch across the sensor results in a complete electrical open.

Figure 23: Surface Artifacts on Kapton

One more result of processing problems is shown in Figure 24. This picture illustrates the effect of excessive heating of the photoresist during sputtering. Because of the excess baking that occurs, it is impossible for liftoff chemicals to completely soften the resist, resulting in incomplete liftoff, and chemical residue on the substrate surface. Since a clean substrate is critical, the residue left behind by excessive baking of the resist is completely unacceptable.

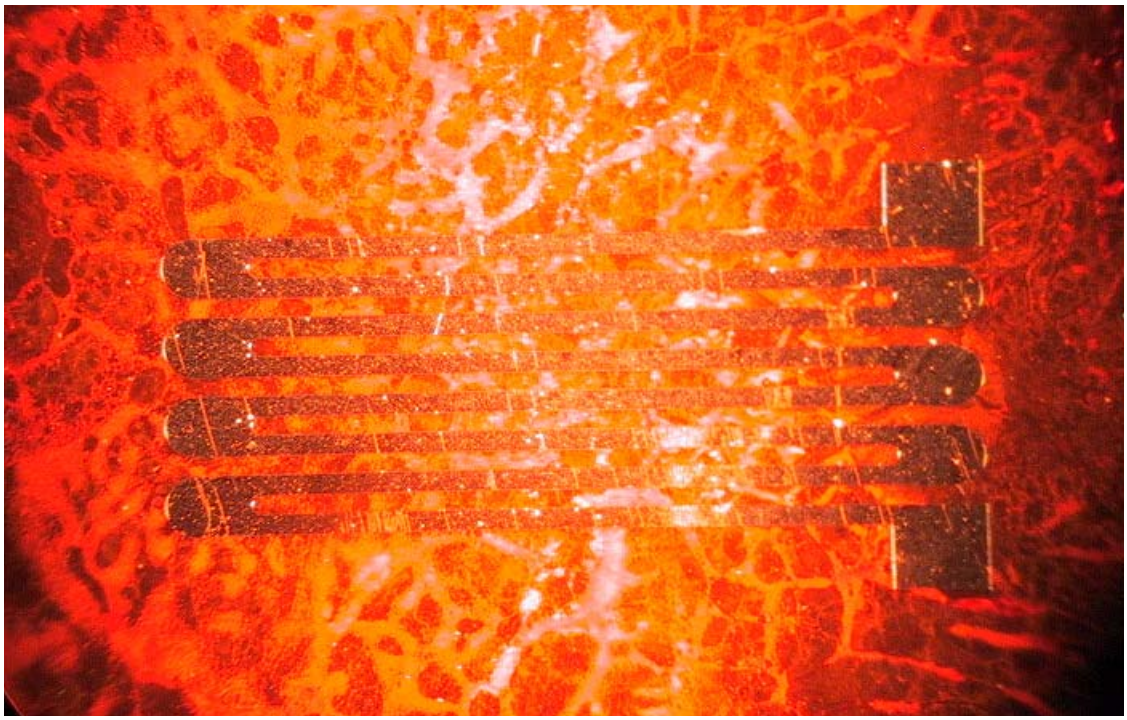

Figure 24: Excessive Baking of Photoresist During Magnetron Sputtering

PLATINUM SENSOR FABRICATION

Platinum has very high strain and temperature coefficients, and is chosen as one element of a temperature sensing pair in the present design layout (parallel to a NiCr sensor having a very small temperature coefficient of resistance). Three specific processing issues were solved in order to successfully fabricate Pt sensors: 1) Processing with Pt metal layers on nonmetallic substrates is well known to result in poor adhesion; 2) metal films in general contain considerable intrinsic stresses due to the deposition process; and 3) Pt etching requires use of a strong acid at elevated temperatures.[12]

To promote Pt sensor adhesion to the Kapton® sheet, the DC Magnetron sputtering process was optimized to reduce film stress, and an adhesion layer was deposited between the Kapton® and Pt layers. Experimentally varying sputtering pressure, and substrate to target distance, and total power (all which affect the energy of species bombarding the substrate), we determined conditions under which the film stress would be tensile, ~zero, or compressive. Then, by first sputter depositing an appropriate TiO_x adhesion layer, a Pt film which can withstand further processing steps has been achieved. Without these critical steps, the Pt films consistently peeled from the Kapton® during photolithographic processing or even upon air exposure after deposition.

Because of the concentrated, heated (~70ºC) aqua-regia etch required for Pt films (aqua-regia is a nitric and hydrochloric acid aqueous mixture), we have utilized a reverse-process lift-off technique for sensor pattern definition. Photoresist is spun and patterned onto the Kapton®, opening only the Pt sensor areas. Then, the Ti adhesion and Pt layers are deposited, and lifted-off by dissolving the photoresist in acetone, leaving only the Pt sensor on Kapton® in the patterned regions. Thus the use of strong acid is eliminated.

The challenge in this step is to keep the photoresist from heating during the metal deposition, causing cracking and polymerization. This has been effectively resolved, after a number of trials, through 2 further process modifications, as listed in the process flow chart (Table III).

A photo of patterned Pt sensors on the 6"x 6" Kapton® sheet from the first prototype array is shown in Figure 25a (Figure 25b is a closer more detailed view of a single Pt sensor). Redesigned to have a resistance of 300 Ω (due to the need to conserve target materials), the 12 sensors here measured room temperature resistance values of 300 Ω, ±5%. In Figure 26, a single Pt sensor fabricated for the second prototype array is indicated (circled in black) and is paired with a NiCr strain rosette. The 2nd generation Pt sensors are also designed to have a 300Ω resistance and are the same thickness as the sensors for the first prototype array, but half the length and half the width.

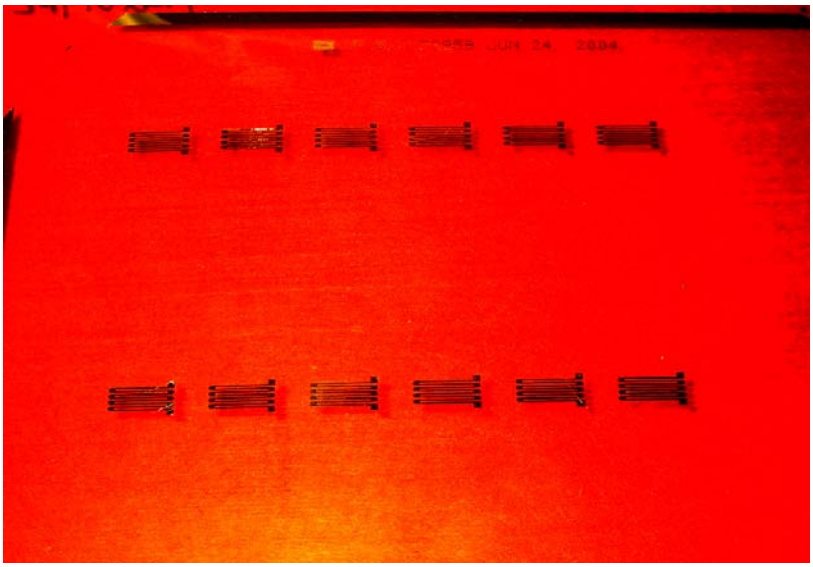

Figure 25a: Pt Sensors on Kapton

Figure 25b: Single Pt Sensor Closeup

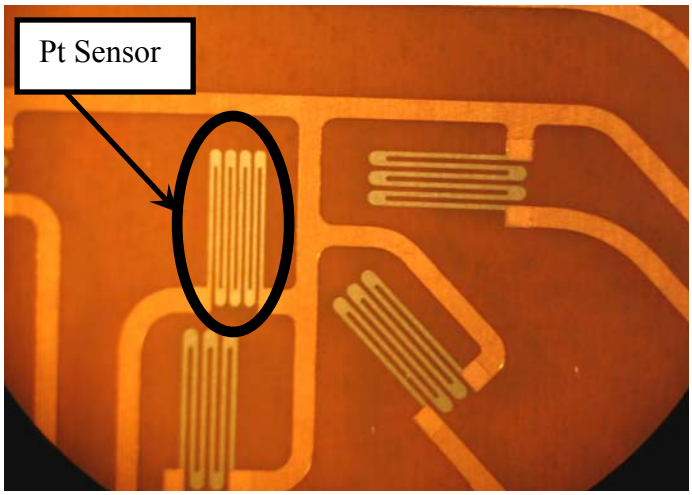

Figure 26: Pt Sensor Within Rosette Pattern

NICHROME SENSOR FABRICATION

The second sensor in the temperature sensing pair, and groups of three sensors forming a strain sensor rosette, are fabricated from NiCr 80 (80% Ni, 20%Cr). Its very low temperature coefficient of resistance is the logic behind this choice. In terms of film processing, NiCr is expected to have better adhesion than Pt, but is easily oxidized.[13] The subsequent layer of polyimide coating used after the first Cu metallization layer should effectively block the oxidation of the NiCr sensors and the Cu conductor lines.[14] Deposition process control to obtain a minimal intrinsic stress, and the use of a Cr adhesion layer, were still required to obtain adherent films. Figure 27 is an enlargement of a NiCr Sensor from the first prototype array. Testing the use of NiCr etchants, we again determined that a lift-off process would be simpler, and produce equivalent results compared to etching. An integrated set of Pt sensors and NiCr sensors from the first prototype array is shown in Figure 28. These also all have good electrical resistance values, most sensors falling within the range of 105 Ohms, ±10% which agrees well with

the original targeted resistance values for the first prototype array. Figure 29 shows the NiCr strain rosette for the second array prototype – the three NiCr sensors are circled in black and indicated by the arrow.

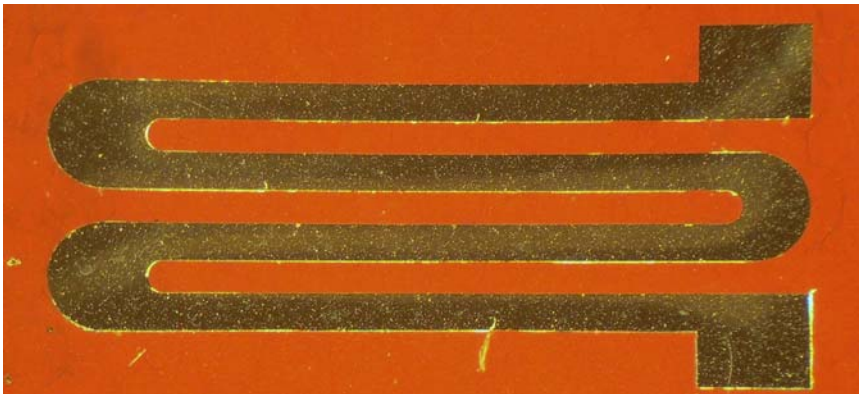

Figure 27: Single NiCr Sensor Closeup

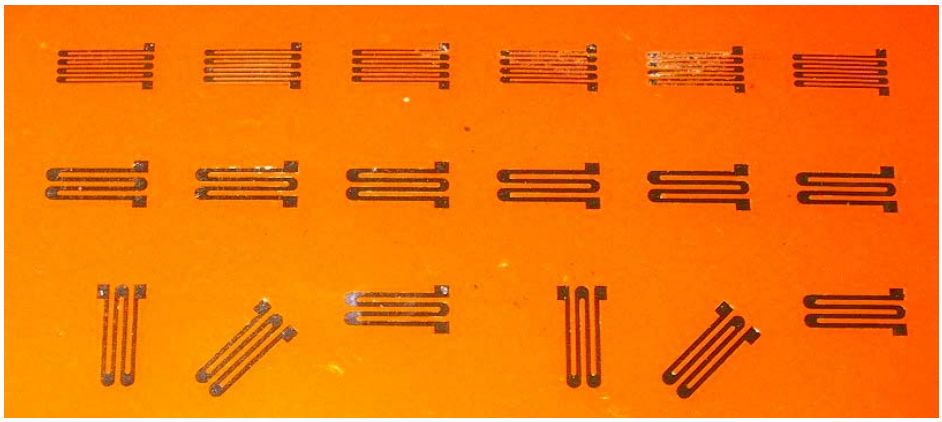

Figure 28: 1st Generation Sensor Arrangement Pt and NiCr

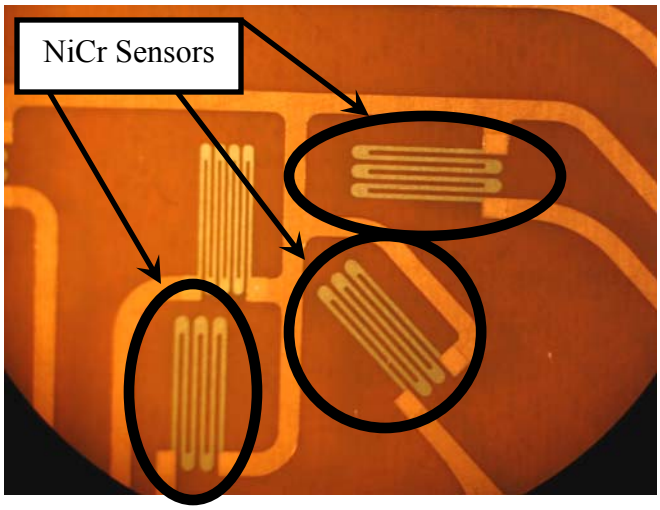

Figure 29: NiCr Strain Rosette, 2nd Generation

INTEGRATED SENSOR ARRAY FABRICATION

Once the individual processing issues for successful fabrication of Pt and NiCr sensors on Kapton® were addressed and resolved, the remaining steps of the array fabrication were developed and refined to complete the process. These steps included the deposition and patterning of Cu interconnects, and polyimide (HD4000 photo-definable polyimide) insulation and passivation layers.

Because the Cu interconnects need to have minimal resistance, it is beneficial to have a large Cu cross-sectional area, and to deposit the purest possible Cu films. Care is taken to minimize the deposition system background pressure during Cu deposition to keep the resistivity low. Cu lines are patterned using a standard wet-etch solution (either FeCl or Ammonium Persufate) which does not significantly attack the Pt or NiCr sensor materials. Between process steps, the array is kept in a vacuum bell-jar to protect from Cu surface oxidation.

To allow for crossing of Cu interconnect lines in the first prototype array and later for the placement of the temperature compensating Pt sensor directly above one of the NiCr Strain sensors (thus integrating temperature and strain sensing into the strain rosette), a multi-level approach is needed. For this purpose, we chose an HD Microsystems photo-definable polyimide (HD4000). The polyimide is spun-on like photoresist, exposed to UV light to photo-define, and cured to a temperature of ~375^{o}C in an inert environment. To minimize the copper and NiChrome oxidation process at elevated temperatures, an enclosed tube furnace with a flowing forming gas (1% H_2 in N_2) atmosphere is utilized. The subsequent layer of polyimide coating used after the Cu metallization layer (or layers) should effectively block the oxidation of the NiCr sensors as well as the Cu conductor lines.[14]

The completed first prototype array design is shown in Figure 30. To enhance distinction of the 1st and 2nd level Cu interconnects, the photo has been taken with the 1st Cu layer coated with polyimide (thus yellowish in color), and the 2nd Cu layer uncoated (thus reflective in the photo). The completed second prototype array design is shown in Figure 31.

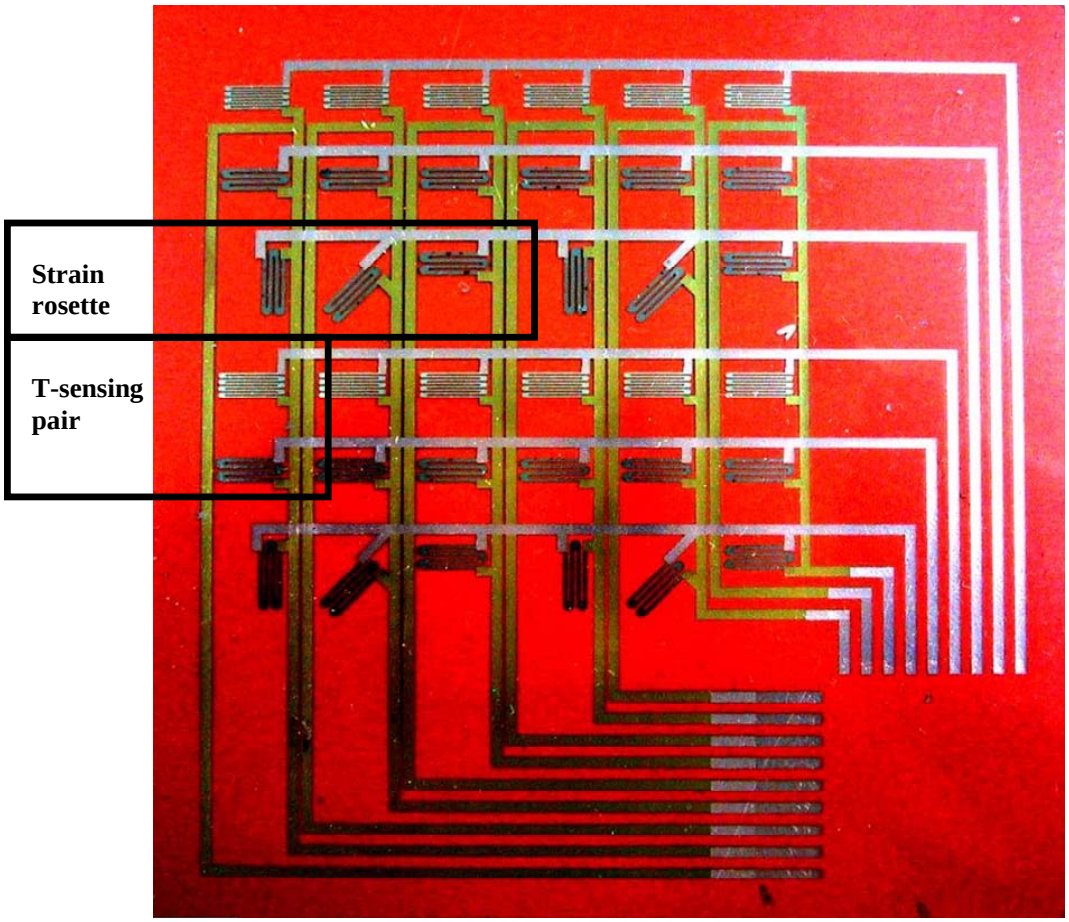

Figure 30: Completed 1st Generation Prototype Array

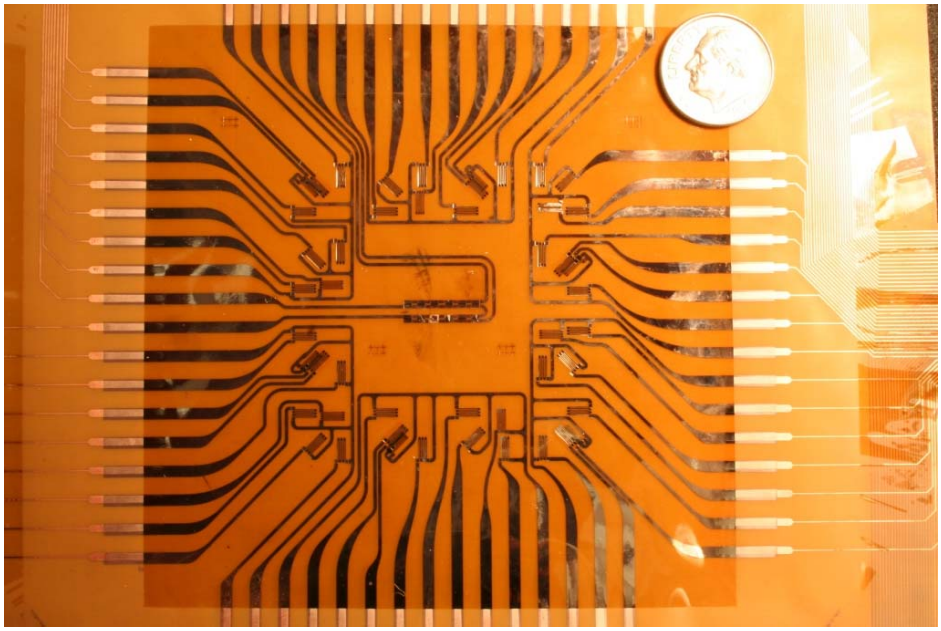

Figure 31: Completed 2nd Generation Prototype Array

The improved 2nd generation temperature and strain sensing array design was completed, and new polyimide patches with integrated copper lines from Cirexx® were obtained. The strain sensor array is designed based on the same principles as used from the project inception, but has been improved upon by using a closer spacing of sensors in the strain rosette, and incorporating the temperature sensing pair as part of the strain rosette. In the interest of reliability the proposed sensor-on-sensor design as illustrated in Figure 33 (with a Pt sensor directly below a NiCr sensor separated by HD-4000) was only used on half of the rosette patterns; this configuration tested the performance-enhanced sensor-on-sensor concept. On the other half, the Pt sensor was placed beside the rosette as illustrated in Figure 32; this reliability-enhanced configuration was used to ensure that fully functional temperature-compensated strain rosettes were available for testing. In Figure 33, the sensor with the darker appearance is one of the three NiCr

sensors of the strain rosette. This sensor appears darker than the other NiCr sensors in part due to being deposited on an additional layer of photodefinable polyimide, which has a slightly smoother surface and is elevated by 5-10μm above the other sensors in the picture. This "darker" NiCr sensor sits directly above a Pt sensor (deposited during an earlier process step) together these two sensors form the RTD parallel pair for temperature compensation.

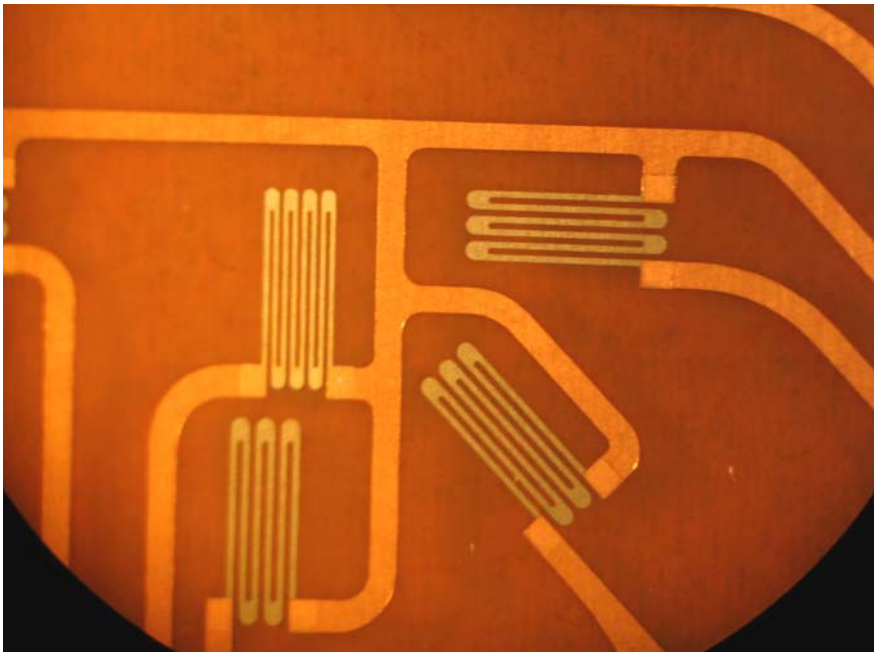

Figure 32: 2nd Generation Strain Rosette, Reliability Enhanced

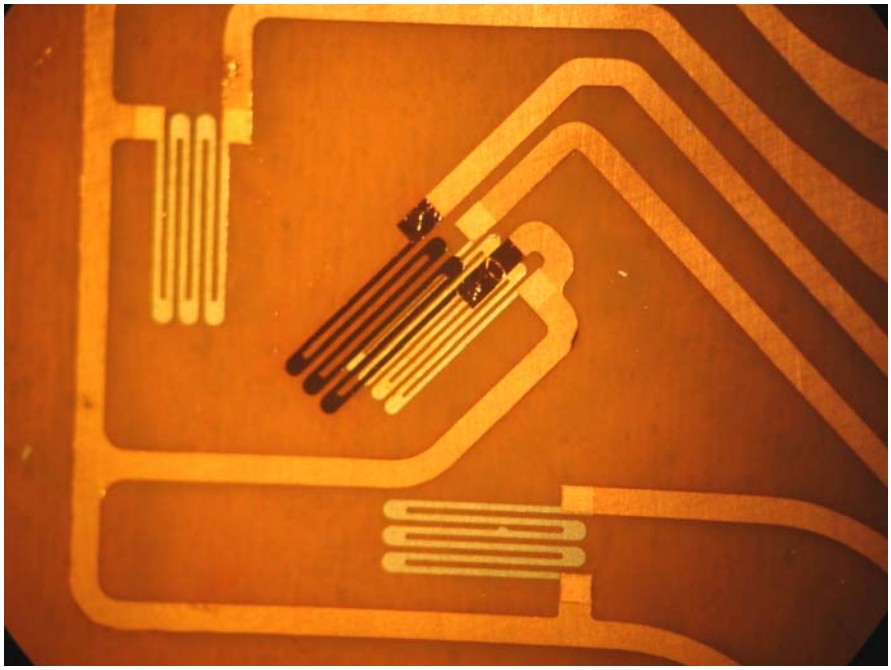

Figure 33: 2nd Generation Strain Rosette, Performance Enhanced

A 3rd generation array was produced very late in the project. This array was tested for initial sensor property measurements and was found to have film resistivities similar to the 2nd generation array. Sensor yield was also similar to that for the 2nd generation array. Figures 34 – 35 below show the completed 3rd generation array, and (for size comparison) all 3 generations of sensor array together. In Figure 35, the arrays are arranged counterclockwise from 1st to 3rd starting at the top.

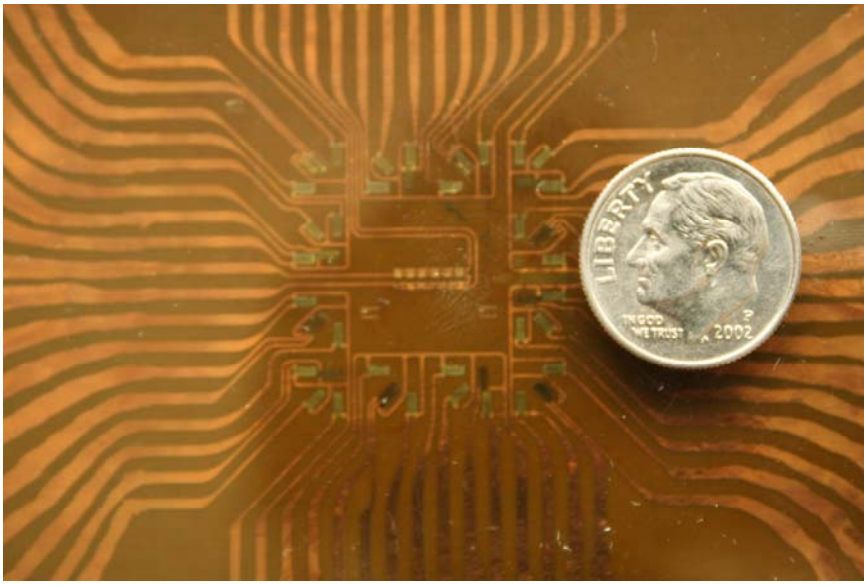

Figure 34: 3rd Generation Array

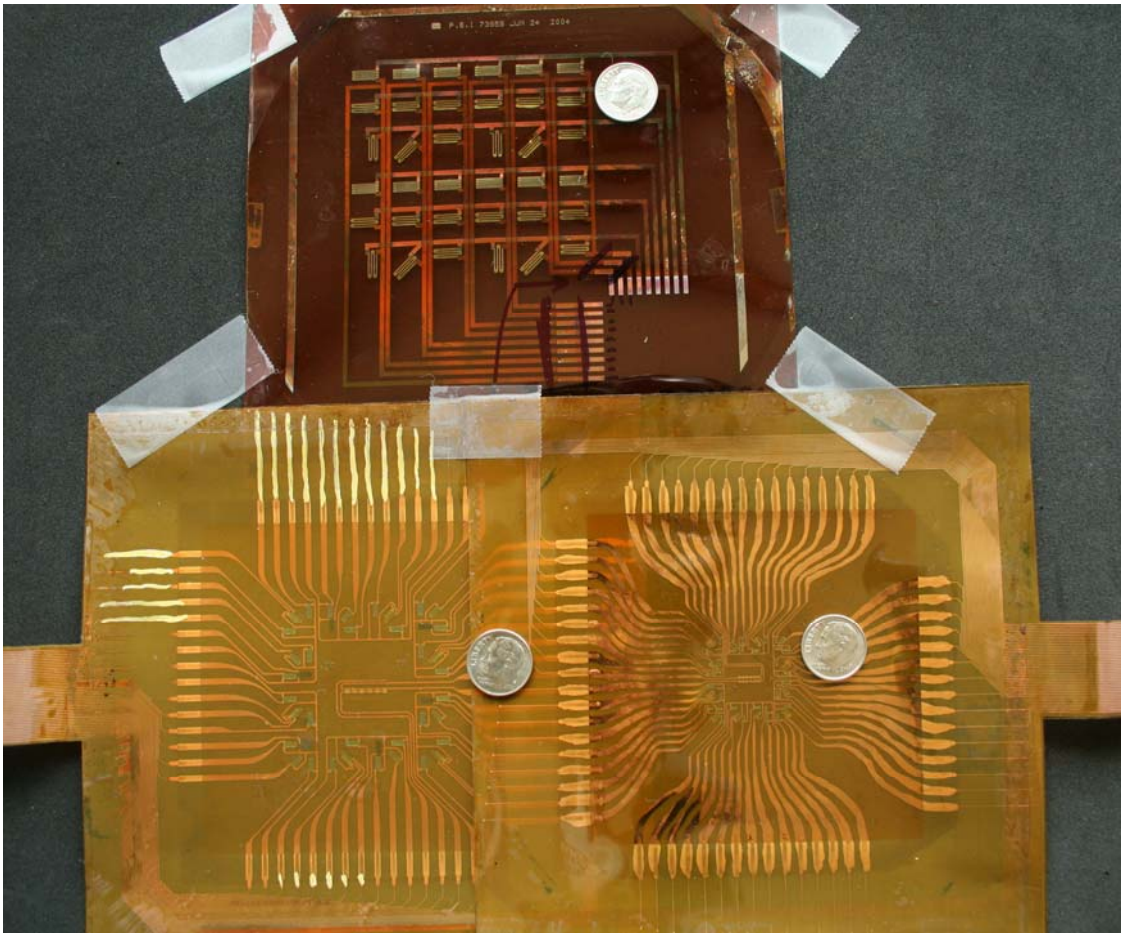

Figure 35: 1st, 2nd & 3rd Generation Arrays (CCW from Top)

Implementation of the new Cirexx® patches presented difficulties due to unexpected issues regarding the Cirexx® patch materials and construction. A problem with the Cirexx® polyimide surface resulted in the failure of many of the NiCr strain sensors. Also, the thickness of the Cirexx® copper pad connection points created open circuits where our own Cu film was unable to connect to the Cu step-interface. These issues are detailed below.

ADDITIONAL PROCESSING CHALLENGES

The liftoff technique was complicated by the fact that the two part photoresist normally used for the liftoff technique proved to be very susceptible to excessive hardening under the deposition conditions required by this prototype fabrication. This challenge was helped significantly by the addition of JSR Electronics NFR016 negative photoresist. With this photoresist it was possible to spin on a fairly thick coating of resist (up to 4μm) with no impact to the 70μm feature sizes on third and smallest array design. One of the useful properties observed in this resist was a "self-shielding" effect where the thickness of the resist actually allowed the resist closest to the substrate to remain somewhat soft, while the resist closest to the UV exposure source became fully hardened. This allowed for the creation of an "undercut" when the resist was developed, allowing the metal film fro the sensor to be deposited through the developed opening in the resist without having any film connection between the patterned sensor and the surrounding resist. This allows for very clean and well-defined liftoff with no torn or jagged edges on the sensors as one would find in some instances of liftoff processing. The clear advantage of this resist is in achieving the sharpness of a two-part "lift-off-resist" with

only a single layer of photoresist. Figures 36a-h depict the formation of an undercut using the NFR016 negative photoresist.

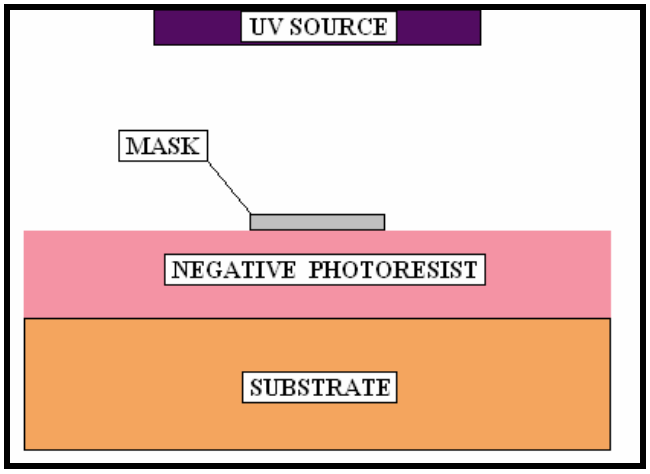

Figure 36a: Undercut Pre-Exposure

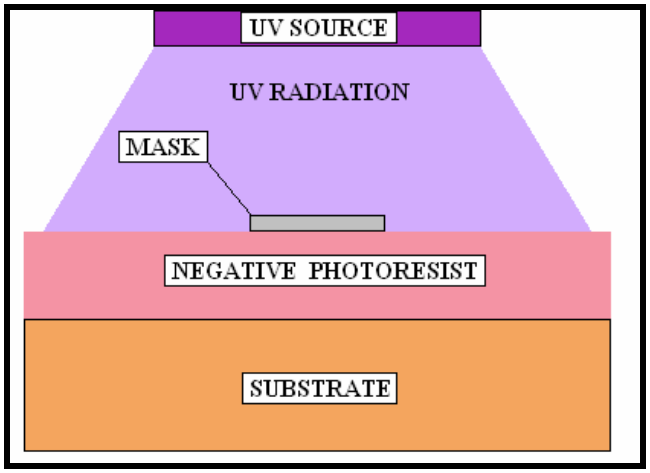

Figure 36b: Undercut Initial Exposure

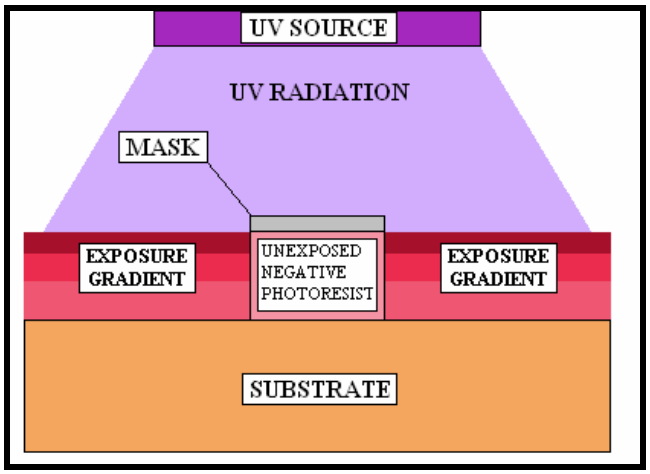

Figure 36c: Undercut Full Exposure

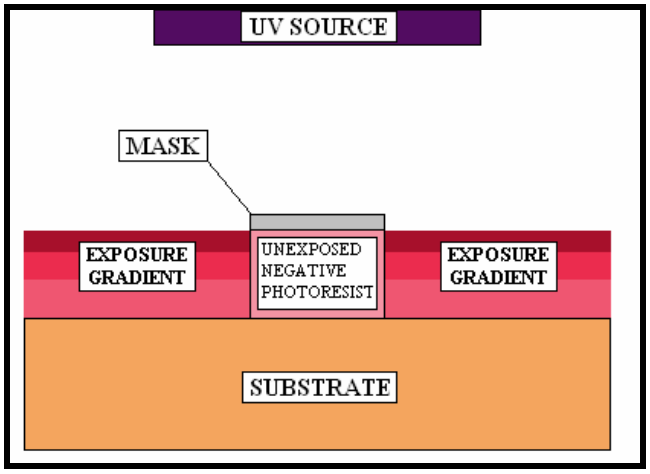

Figure 36d: Post-Exposure

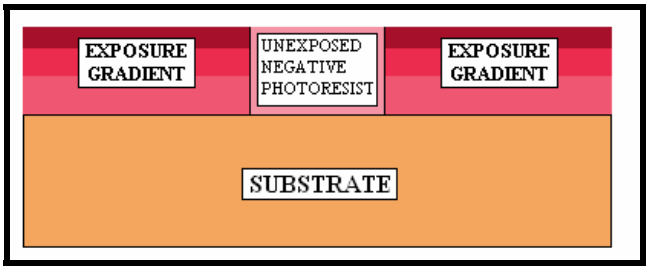

Figure 36e: Pre-Develop

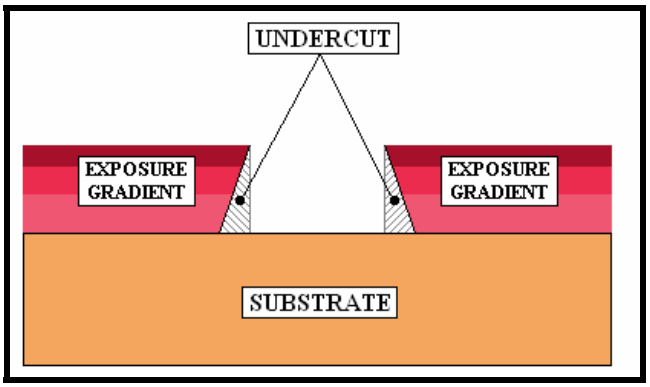

Figure 36f: Develop Showing Undercut

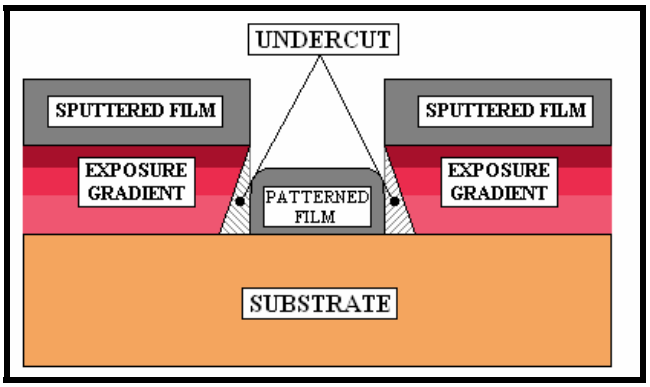

Figure 36g: Metal Film Deposition with Undercut

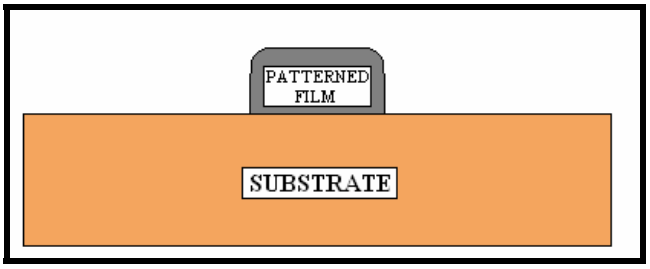

Figure 36h: Film Liftoff Leaving Patterned Metal

The use of the Cirexx® patches was intended to make final product testing more reliable because of the integrated copper lines terminating at a ribbon-cable end 'tail' for easy electrical connection. However, this resulted in a number of unexpected new

processing challenges in comparison to the fabrication of sensor arrays on Kapton® sheets.

One significant problem encountered was a process temperature limitation. We require a process temperature of ~375°C to fully cure a spin-on photodefinable polyimide insulation layer, and ideally a temperature of 300°C or greater to stabilize the NiCr film properties (which the Kapton® sheet acceptably withstands). Although the Cirexx® pads are defined as 'all polyimide', they are a triple laminate of polyimide layers joined with adhesive. These patches blacken, harden, and wrinkle at temperatures above ~200°C due to temperature limitations of the adhesive which bonds the polyimide sheet layers. We were able to obtain Cirexx® patches of an alternate design (single-layer construction, without adhesive), and carry on with fabrication at somewhat lower process temperatures because the Cirexx® polyimide is less thermally robust than Kapton®. It is important to understand that when working with a photodefinable polyimide, failure to reach the fully cured state will yield less than ideal properties and result in a polyimide with inferior electrical and chemical properties as compared to those achieved by fully curing.

A second major problem encountered deals with roughness in the Cirexx® polyimide sheet surface. The Cirexx® polyimide patch is fabricated from a copper-clad sheet, patterned and etched to leave Cu interconnects. The surface of the polyimide is roughened slightly prior to the copper-cladding process, which leaves rows of "sharp ridges" in the polyimide surface. These ridges are sufficiently deep to initiate cracking in the NiCr sensors, thus resulting in failure of the sensor due to open circuit. To solve this problem, we have introduced a new material and process step into the sensor array fabrication. It was decided that a layer of spin-on polyimide would be the best solution to

the Cirexx® patch surface roughness. After many attempts to introduce a standard spin-on polyimide (DuPont/Hitachi Microsystems PI-2525) as a base layer, we determined that only the original (and very expensive) photo-definable polyimide would withstand the required processing steps, produce a suitably smooth surface finish and promote metal film adhesion. We are now using another layer of HD-4000 spin-on polyimide to serve as a base leveling layer which the sensor array is to be fabricated upon. This is a self-leveling layer which will offer a smoother surface (similar to the original Kapton® patches). An additional benefit of the spin-on polyimide is that it was specifically designed to promote adhesion of deposited metal films. Figure 37 shows an image of the single-layer Cirexx® patch, with our spin-on polyimide (HD Microsystems HD-4000) base layer.

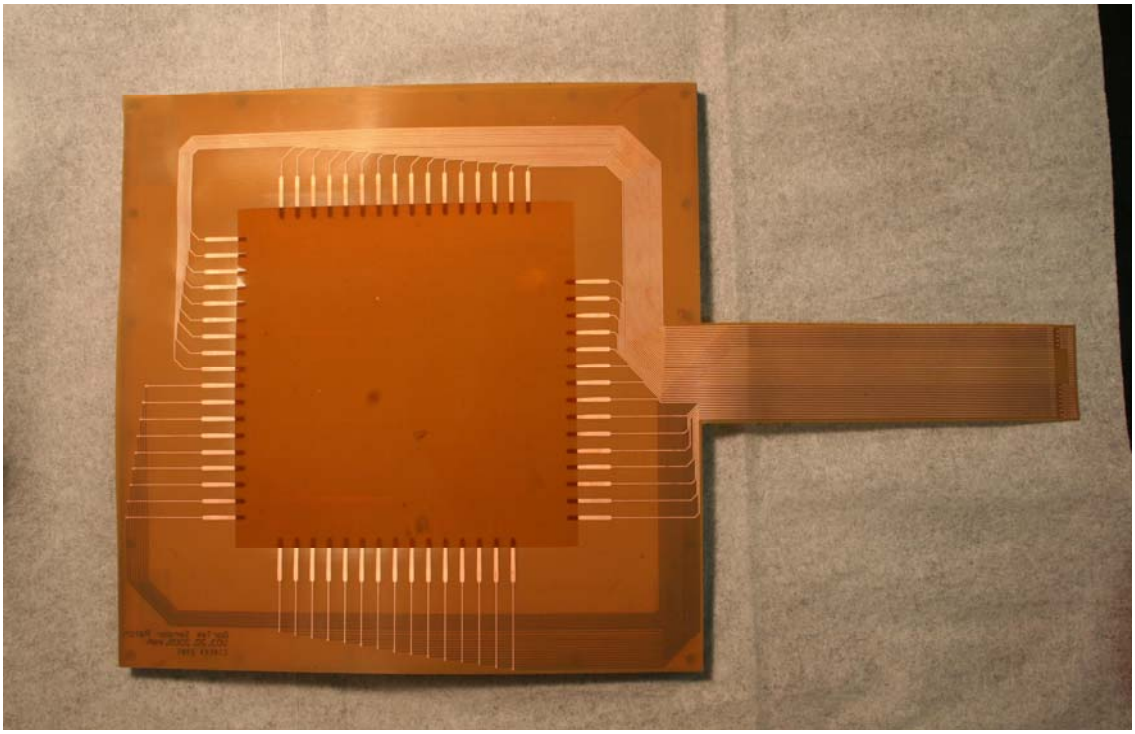

Figure 37: Cirexx Patch Substrate for 2nd Generation Array

A third major difficulty involves connecting thin film copper interconnects to the thick copper pads on the prefabricated Cirexx® patch. Our copper lines are a few microns thick, while the Cirexx® pads are about 30μm in thickness. This step height makes the connection of layers difficult not only because of the large step-height, but also because of a shadowing effect at the edges of the Cirexx® Cu pads during sputtering such that the sputtered film Cu would usually not make physical contact with the thick film Cu pad edge – the result was an open circuit from the array to the Cirexx® copper interconnect lines. We were able to solve this problem by using a mild etch of the Cirexx® Cu pads with ammonium persulfate to round the edges of the pads and thin them some. This process has greatly improved the reliability of the copper film to copper pad connection. Figure 38 shows the technique used to etch the thick film Cu pads. This technique did not use any masking because of the additional incurred time and cost of making another photo mask.

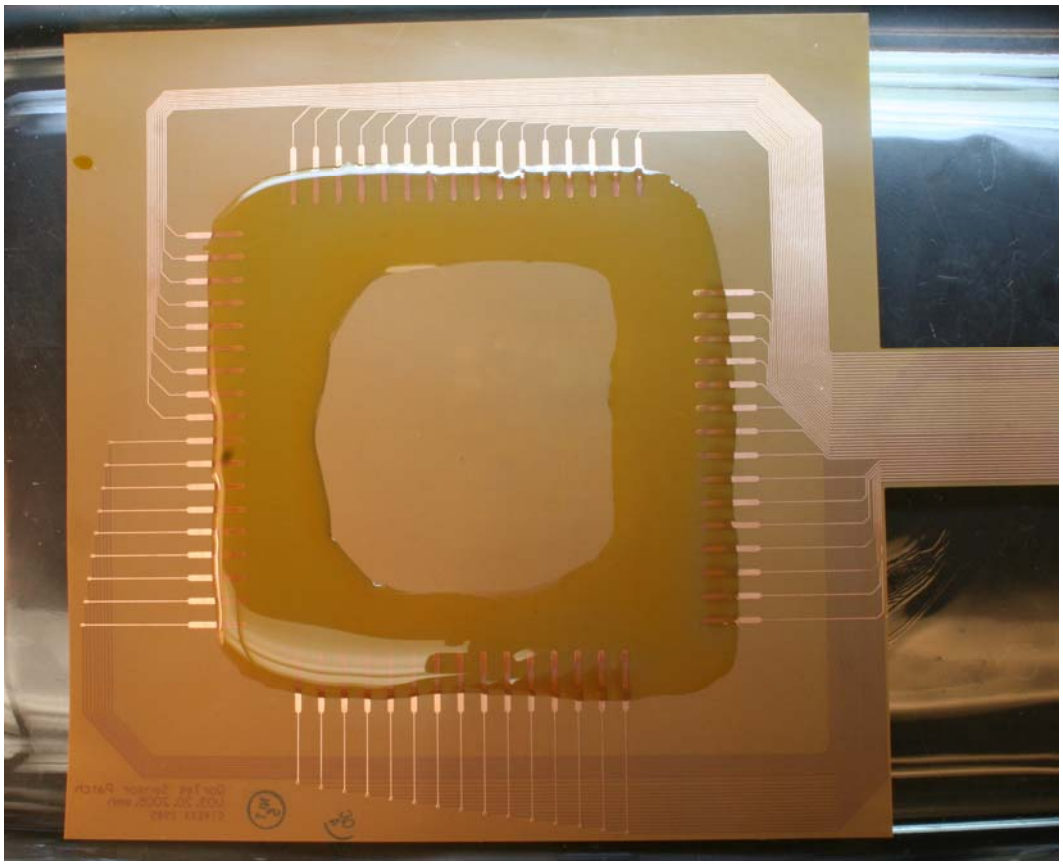

Figure 38: Etching of Thick Film Cu Pads

Another processing challenge that had to be overcome was the irregular, asymmetric shape of the Cirexx® patch. This was a significant challenge as the primary means of patterning our sensors was a photolithographic technique and required the use of spin coating to distribute the photosensitive chemicals evenly over the patch surface. This was accomplished by taping the "tail" of the patch to the bottom of the patch and then taping the patch itself to a 6' diameter wafer. The success of this technique is evidenced in Figures 39-41, which show the patch at rest on the spin coater (39) during initial spin motion (40) and at 2500+ RPM (41).

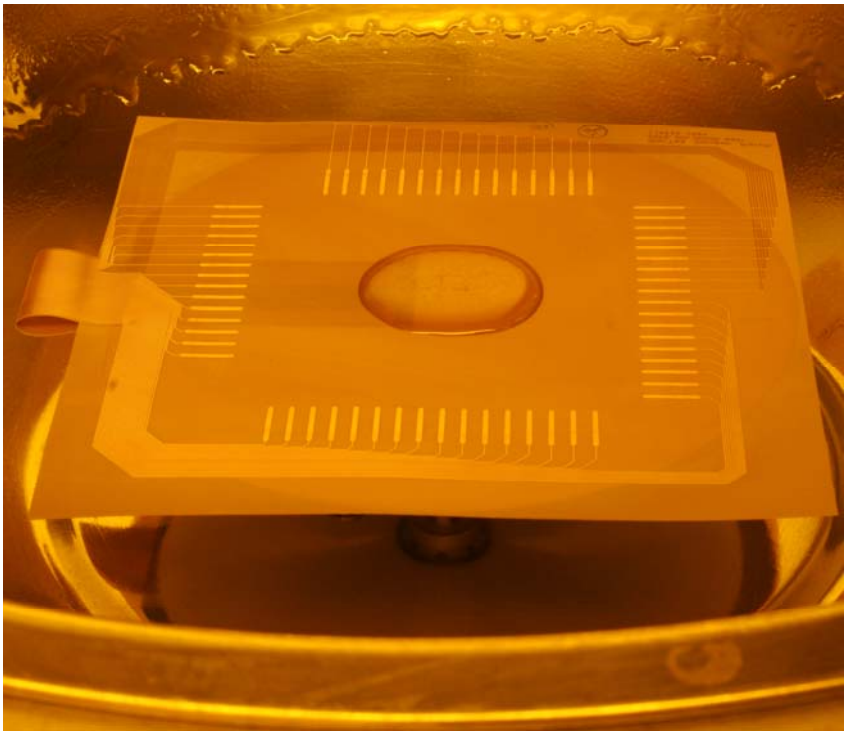

Figure 39: Photoresist on Cirexx Patch on Spinner at Rest

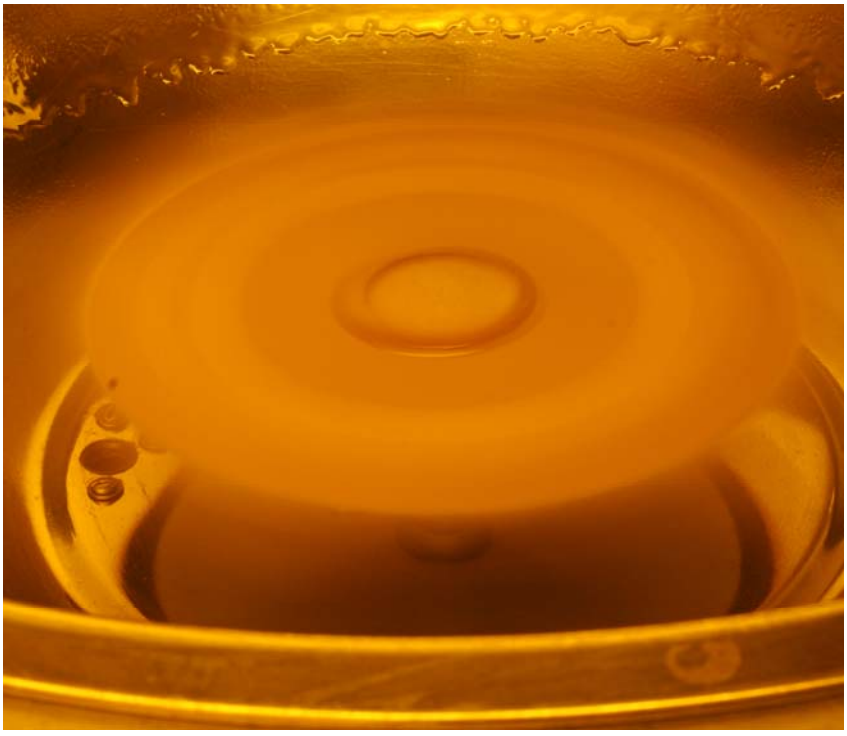

Figure 40: Photoresist on Cirexx Patch on Spinner During Initial Spin Motion

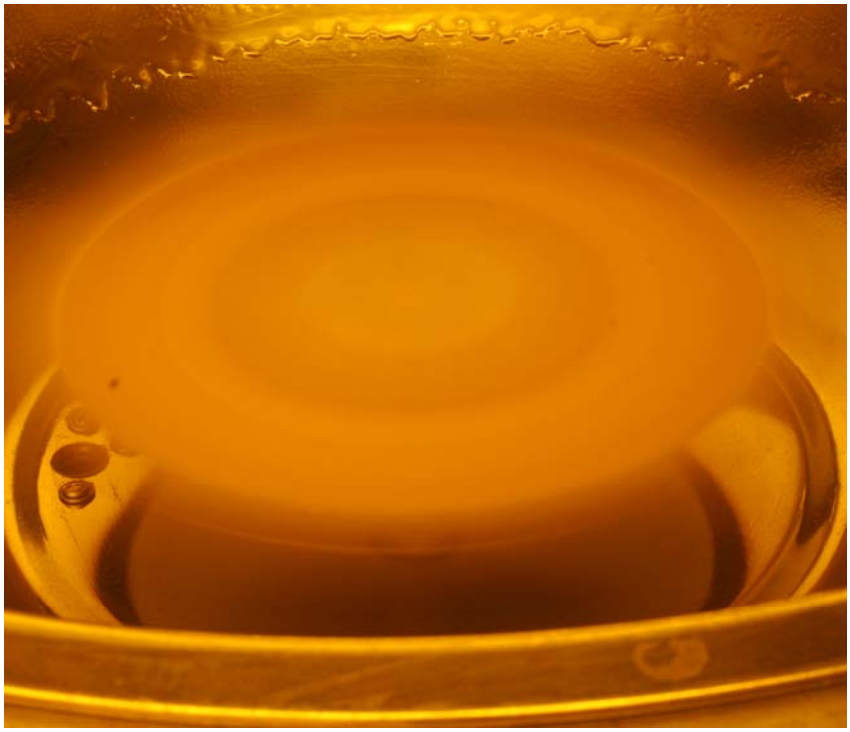

Figure 41: Photoresist on Cirexx Patch on Spinner at 2500+ RPM

ELECTRICAL TESTING

With Cu interconnects, electrical testing of actual sensors on the first array was performed where previous testing had been only on larger, straight lines which had not been subjected to all the process steps required of total array fabrication. Because of the problems with the Cu interconnect layout in the first prototype array, the 18 Cu lines on that array allow only 12 sensors to be tested. Additionally, physical alteration of interconnects by scratching open specific Cu interconnects is required to make even this possible. The sensors described here were measured using an Agilent 34401A, 6½ Digit 34401A multimeter, using lead wires attached to the Cu contact pads of the sensor array using silver paste and silicone adhesive for mechanical strength. The entire array was

placed on a covered hot plate, with an adjacent type K thermocouple for temperature measurement/control.

The response of an array of sensors to temperature change (from ambient room temperature (RT) to 180^{o}C and back to RT) has been measured. Figure 42 shows a comparison of the temperature response of a Pt and NiCr sensor on the same sensor array. Note the goal resistance of 300 Ohms for both sensors, and the very different temperature response, as desired. Figure 43 shows the results of 6 sensors from the same sensor array, again measuring from the ends of the Cu interconnect lines. The data is plotted as resistance divided by the extrapolated 0^{o}C resistance, so that the slope of the line represents the TCR value. The calculation of TCR is accomplished as follows:

$\alpha = \left(\frac{R_f - R_o}{R_o \left(T_f - T_o \right)} \right)$, where α is TCR, R_f is final measured resistance, R_o is initial measured resistance, and T_f and T_o are final and initial measured temperatures, respectively. Represented are 3 Pt sensors and 3 NiCr sensors. The Pt sensors show excellent linearity, and behave nearly identically, with a TCR value of ~0.0028 Ω/Ω/C^{o}. This is less than the value for very pure Pt (0.00385), but TCR values of sputtered sensors are affected by impurities and grain size, so the obtained TCR values are within reason given the deposition technique and conditions. Figure 44 depicts the testing setup used to measure temperature response of the array sensors.

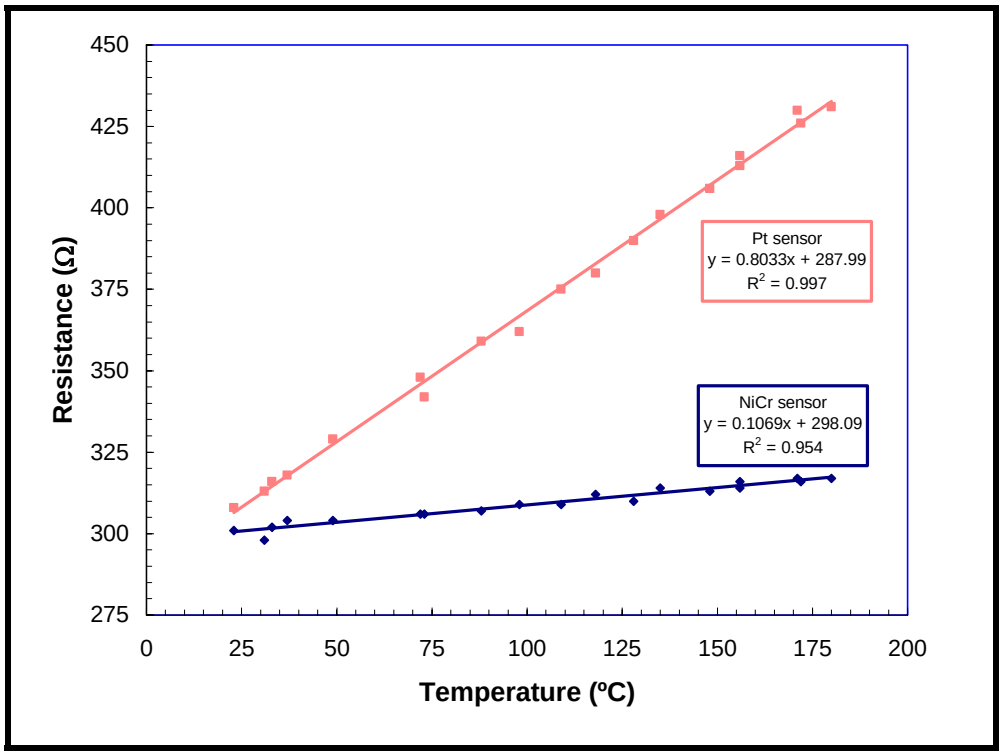

Figure 42: Temperature Response of Pt and NiCr Sensors from Single Array

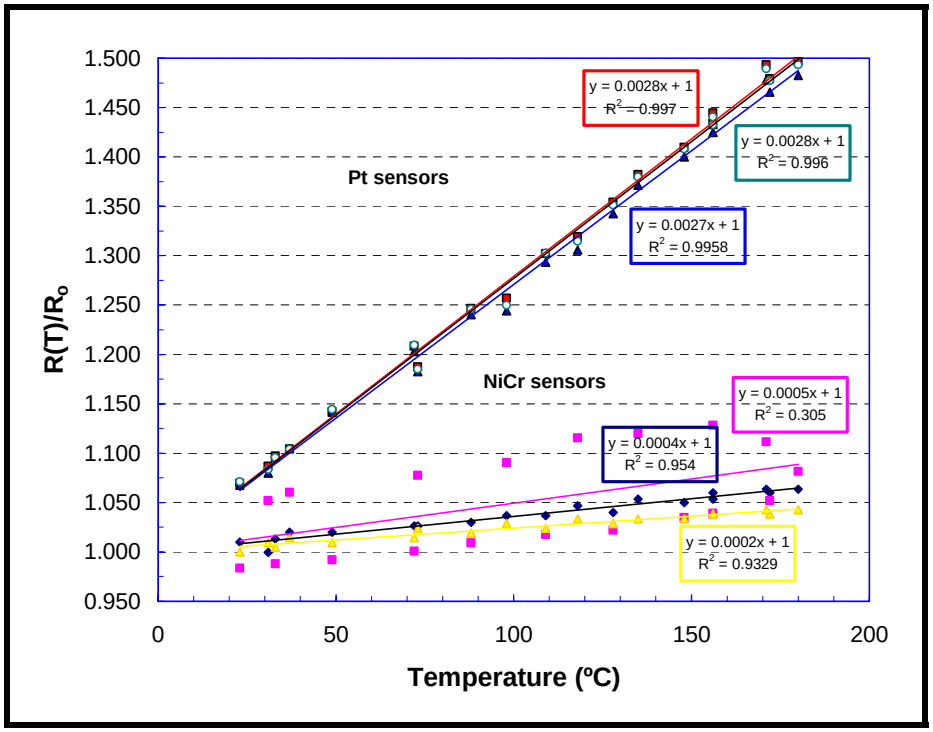

Figure 43: Temperature Response of Pt and NiCr Sensors from Single Array

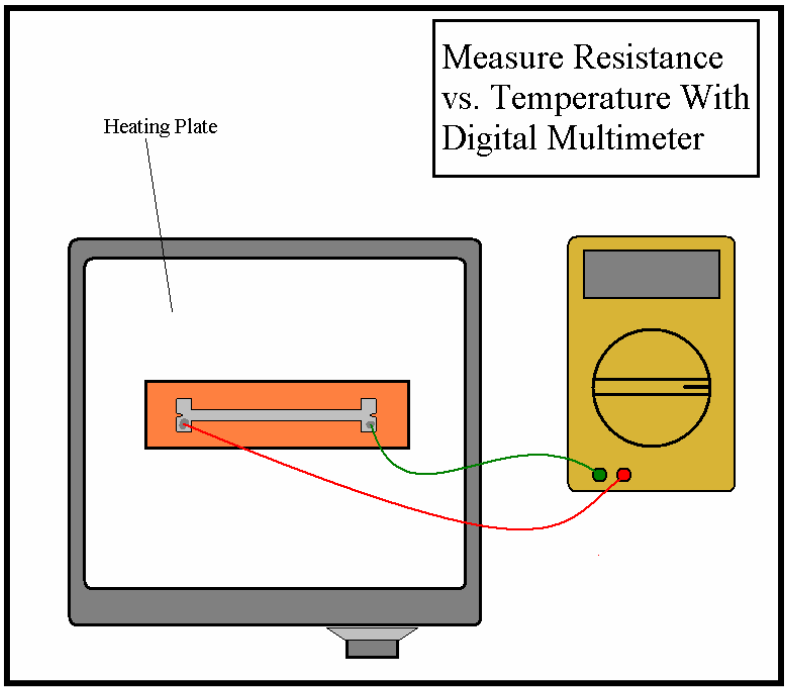

Figure 44: Temperature Response Measurements

The TCR values for NiCr are seen to be a factor of ten lower than Pt, with values from 0.0002-0.0005 for the sensors measured here. This provides the needed ability to distinguish temperature from strain, since the NiCr is virtually temperature independent. However, as revealed in Figure 43, the NiCr sensors show more variability from sensor to sensor, and one in particular shows a very nonlinear temperature response. It is known that the TCR of NiCr is very processing-dependent,[15] as oxygen impurities can change the TCR from positive (low pO_2) to negative (higher pO_2). Efforts to enhance NiCr uniformity will have to be increased to minimize TCR differences.

In Table VII below, we include resistance readings from sensors (measured from the patch tail) on one second-generation array, at RT (~22°C) and at 113°C. These resistance values are 2-pt measurements which include copper line resistances. Measurements of the common '3rd' lines indicate a Cu line resistance of 6-10 Ohms at

RT, and 9-13 Ohms at 113°C. Included in the table is the TCR as-measured. Note that Pt sensors have very small scatter in resistance and TCR values, and TCR values are an order of magnitude higher for Pt than for NiCr, as expected. The Pt TCR values of ~0.0024 /°C are lower than that of bulk Pt (0.00385), presumably due to the thin-film microstructure and effects of impurities. Some scatter in the NiCr resistance and TCR values is observed, revealing the sensitivity of NiCr to impurities during deposition, and air exposure. The TCR of NiCr is known to be a function of Ni/Cr ratio, and amount of Oxygen impurity. High-temperature post-process anneals are known to stabilize NiCr against atmospheric reaction. Nevertheless, the effect of choosing sensor pairs materials of varying properties is demonstrated.

Table VII: Various Measured TCRs of Sensor from Single Array

Sensor Group/#	R @ 22°C (Ohms)	R @ 113°C (Ohms)	TCR /°C
Pt I-3	183	219	0.0023
Pt II-2	190	229	0.0025
Pt III-3	186	224	0.0024
Pt IV-7	173	209	0.0024
Pt V-2	170	205	0.0024
NiCr I-1	133	138	0.00042
NiCr III-6	160	146	-0.00095
NiCr IV-1	148	152	0.00030
NiCr V-1	156	160	0.00028
NiCr V-6	350	350	0.000

Electrical testing of the arrays indicates that completed arrays have only ~30% working sensors, revealing unsolved issues regarding array fabrication that we will not have the opportunity to resolve in this project. The 'open' sensor readings are failures that are undoubtedly due to contact/connection issues between the deposited Cu interconnects and the sensor or between the Cirexx® Cu contact pads and the sputtered Cu – however, the exact cause and nature of the problem is not yet known.

The functional sensors have exhibited thermal resistivity responses very close to the expected values, with the Pt sensors having ~10X more temperature sensitivity than the NiCr, thus providing for temperature and strain determination. Strain testing (tensile

stressing on a conventional strength-testing instrument) has not given as reliable/repeatable results as the temperature testing; we believe this is due to the viscoelastic properties of the polyimide base layer combined with the previously stated material properties issues related to residual strain, grain size and oxygen impurities. The basic strain response characteristics, however, show the expected design trends. We have produced 6 complete 2nd generation sensor arrays with sufficient functional sensors to perform initial strain and thermal response testing.

Overall 2nd generation sensor array patch evaluation

Initial array evaluation requires resistance testing of individual sensors from the Cirexx® tail edge contact points. In this initial testing we found that only ~25% of sensors on a given array have the expected resistance values. Failed sensors give open readings; which indicate a likelihood of failure at metal/metal contact points (either deposited Cu to sensor contact, or to Cirexx® Cu) or of cracking-related problems. Visual inspection has not revealed the origin of this contact problem. Figure 45 illustrates the final design/fabrication of the 2nd generation array prototype.

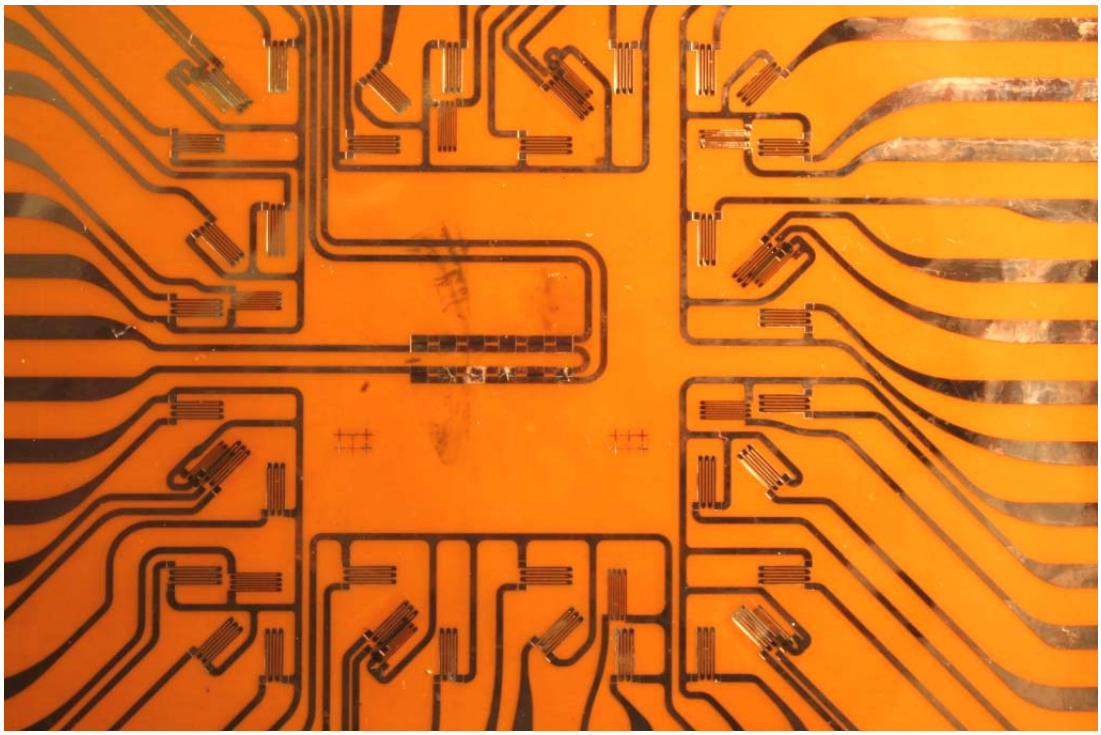

Figure 45: 2nd Generation Array Closeup

2nd generation sensor array temperature response

The temperature response of the working sensors has been determined by measuring sensor resistances as the entire array patch is heated uniformly on a large metal plate, enclosed to maximize temperature uniformity. A type-K thermocouple is used to measure the temperature of the assembly, while individual sensor resistances are measured. The temperature response for one sensor array set is shown in Figures 46 and 47. In Figure 46 the NiCr sensor response is shown, and in Figure 47 the Pt response. One complete array contains 36 NiCr and 12 Pt sensors; Figures 46 and 47 reveal the working sensors from one particular array patch designated Cirexx® NL-08.

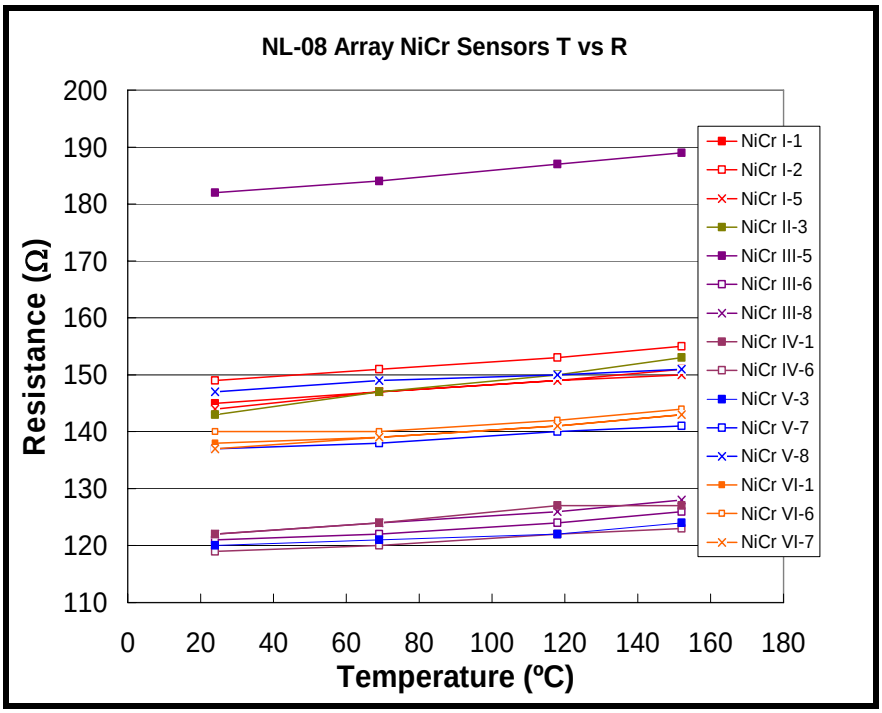

Figure 46: 2nd Generation Array NL-08 NiCr Sensor Temperature Response

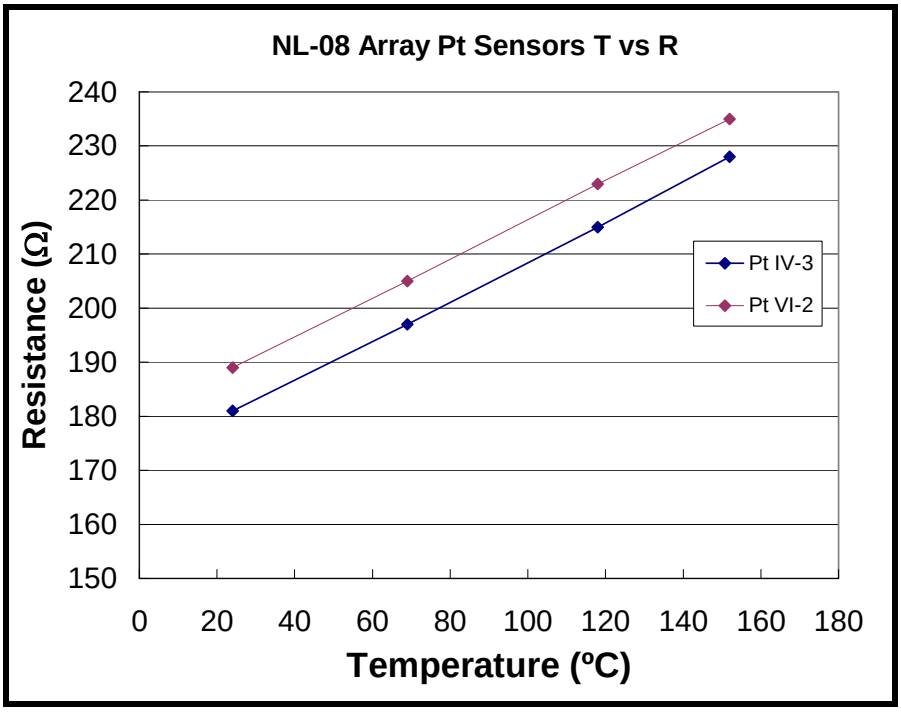

Figure 47: 2nd Generation Array NL-08 Pt Sensor Temperature Response

From the obtained data, the temperature coefficient of resistance $(R_T-R_0)/R_0/(\delta T)$ is found to be ~$2.2x10^{-4}$ Ω/Ω/°C for NiCr, and $2.0x10^{-3}$ Ω/Ω/°C for Pt. This large difference indicates that temperature and strain response can be separated because of the material property difference, as designed. This holds true regardless of the difference in strain response of the two materials.

2nd generation sensor array strain response

We have performed strain testing on the sensor array in a standard tensile testing instrument. Clamping opposite sides of the array between aluminum bars coated in Plastic Welder™ epoxy, we have applied up to about 1.8% strain to the patch, measuring resistance at discrete steps in-between. During the measurement time, it is observed that the force needed to strain the patch decreases, indicating a viscoelastic response from the polyimide base material. It is presently uncertain how this may affect the local sensor strain. However, this should not be an issue for a patch adhered to a solid surface. A basic representation of the testing configuration for strain measurements is given in Figure 48.

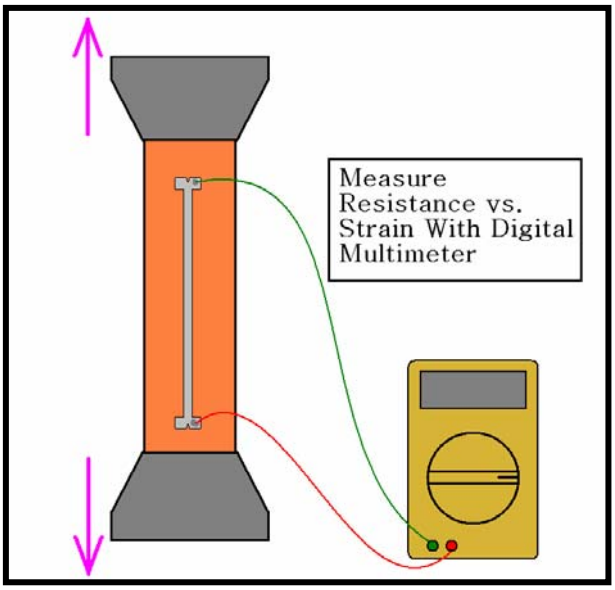

Figure 48: Strain Response Measurement Apparatus

An example showing Pt sensor strain behavior is given in Figure 49. The arrows next to the sensor designation indicate direction with respect to applied stress (↑ indicates the applied strain direction). Although the data is very non-linear and scattered, general trends appear as expected. For example, sensor VI-5 is parallel to the applied stress, and thus should give a positive response, as it does. Most of the others are 45° from the applied stress, and should thus give lower responses (divided by $\sqrt{2}$) but still positive responses.

A key indicator of performance is revealed by sensor V-5. This sensor is perpendicular to the applied stress, and ideally would give no strain response. However, in our test setup (with clamps on only the two tensile stressed ends), stretching the polyimide would produce a contraction (compression) perpendicular to the applied stress, thus the observed drop in resistance for that sensor is explicable.

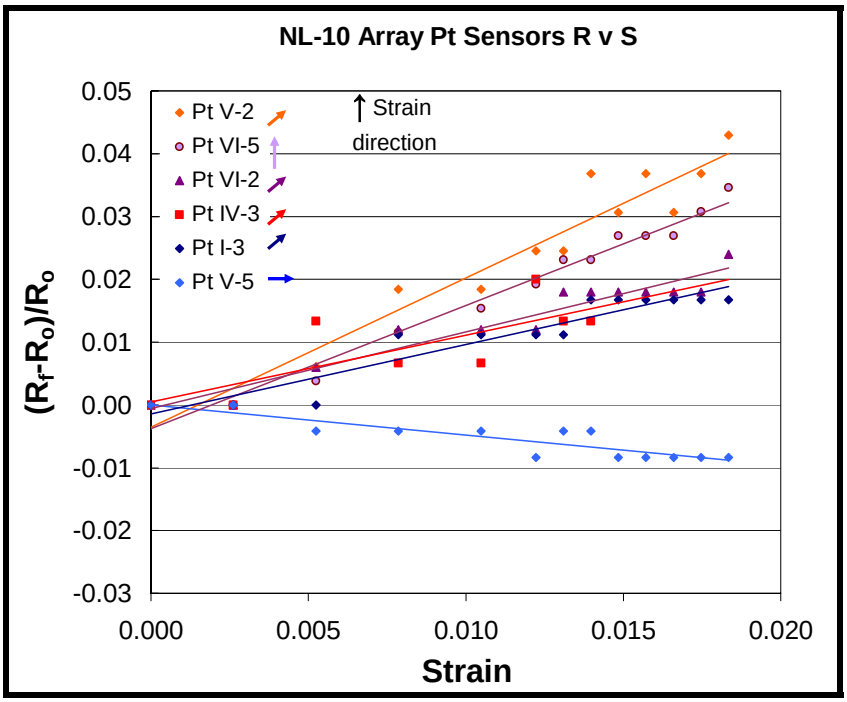

Figure 49: 2nd Generation Array NL-10 Pt Sensor Strain Response

The strain data reveals that for Pt, the gauge factor (or strain sensitivity) is only about 1.5-2.0, whereas it is 6.0 for bulk Pt. Data for NiCr sensors (not shown) is similarly noisy, and reveals (averaged) gauge factors of around 1.0, less than the expected 2.0-2.2 for NiChrome. We expect that array testing by adhesion of the patch to a solid surface will result in less uncertainty in the strain response behavior.

As a reminder, the calculation of gauge factor (GF) is accomplished as follows:

$$GF = \frac{\left(\frac{R_f - R_o}{R_o}\right)}{\left(\frac{L_f - L_o}{L_o}\right)}$$, and can be re written as $$GF = \frac{\left(\frac{R_f}{R_o} - 1\right)}{(\varepsilon)}$$ where R_f is final measured resistance, R_o is initial measured resistance, and L_f and L_o are final and initial measured temperatures, respectively and ε is strain.

Figures 50 and 51 show the most recently collected TCR data from one of the prototype arrays. Figure 50 represents the NiCr data and Figure 51 represents the Pt data. This data has the best agreement with literature values for TCR to date and is both consistent and repeatable. Figures 52 and 53 respectively represent the NiCr and Pt Gage factor data for the same array. This data has been plotted with linear regression to give an averaged Gage factor (Strain Sensitivity) and in the case of Platinum especially, we do not believe that the average gage factor represents the true material property. In the case of platinum, the gage factors represented are all oriented at 45º angles to the strain, except for sensors III-7 and VI-5, both of which are in line with the applied strain. Here it is important to address two issues. First, the variation between the two in-line sensors and the 45º sensors is *roughly* a factor of $\sqrt{2}$. Second, we believe that the reason that the two in-line sensors gage factor is lower than both the literature value *and* the best that has been achieved at NCSU during this project is two-fold. Part of the problem is believed to be in the elastomeric response of the polyimide. We believe that in straining some portions of the polyimide patch strain at different rates with respect to others. Another part of the problem is potentially in the nature of the Pt sensors – specifically their adhesion. The method used to promote adhesion between the polyimide and the Pt sensors (a thin layer of adhesion metal sputtered prior to Pt deposition) was not ideal. In our system it was necessary to remove the array from vacuum to change targets between sputtering the adhesion layer and Pt. This was unavoidable and allowed oxidation to form on the adhesion layer. This could be a contributing factor to the less than ideal performance of the Pt sensors in strain testing. One additional complexity in analyzing the Pt strain data is that all but the in-line sensors are constructed using the

photodefinable polyimide to allow the Pt sensor to be placed directly above a NiCr sensor. This also could account in part for the discrepancy in data. What is clear from the data is that even though the applied strain was essentially uniform, the electrical response of the sensor was not. This indicates that the sensor is in fact experiencing an electrical strain response, and in that sense is functional; however, the strain response is non-uniform, indicating that a material condition – likely either sensor/substrate adhesion, the polyimide strain response or a combination of the two – must be addressed and optimized to affect the best response of these sensors to strain.

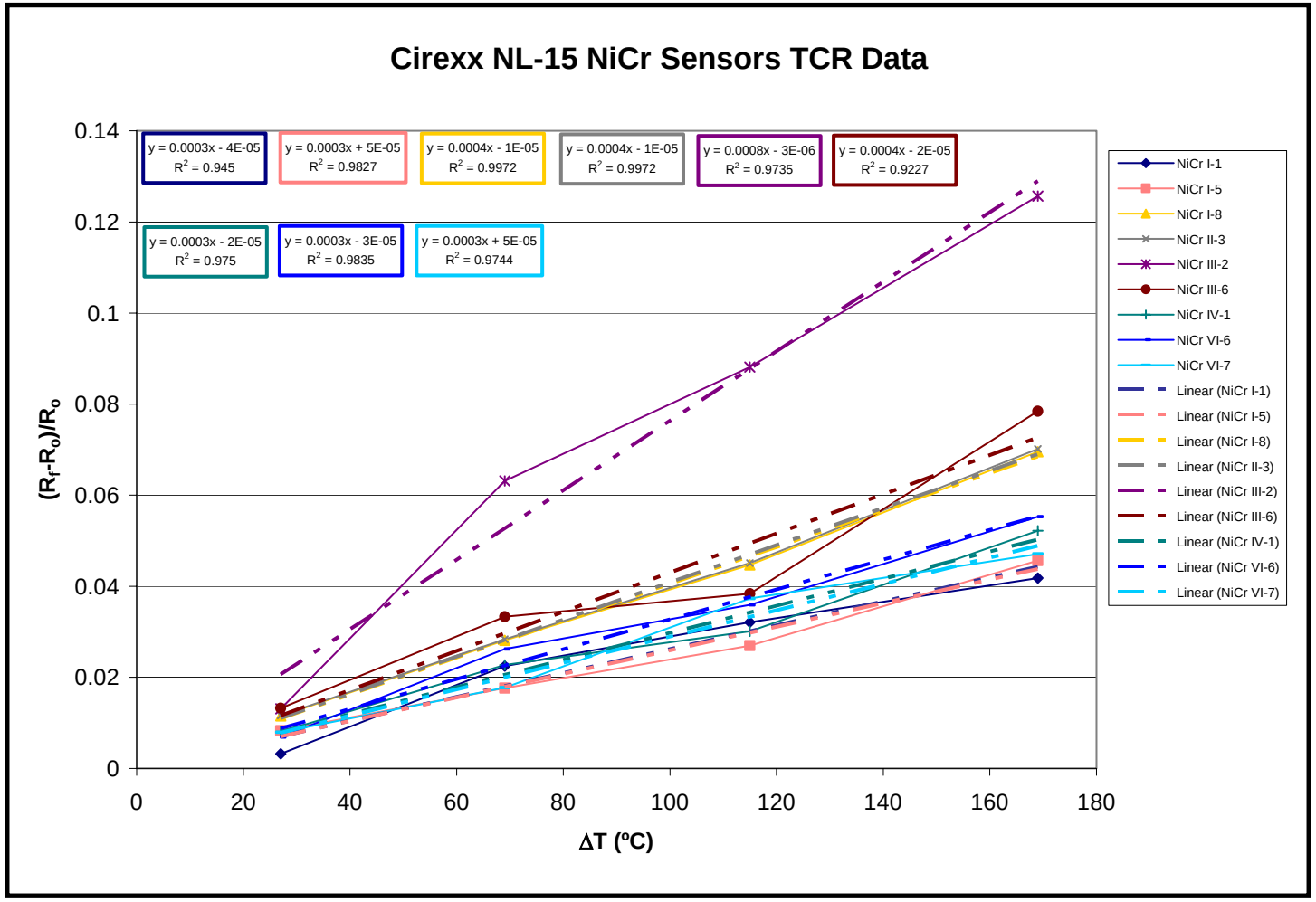

Figure 50: 2nd Generation Array NL-15 NiCr Temperature Response Including TCR

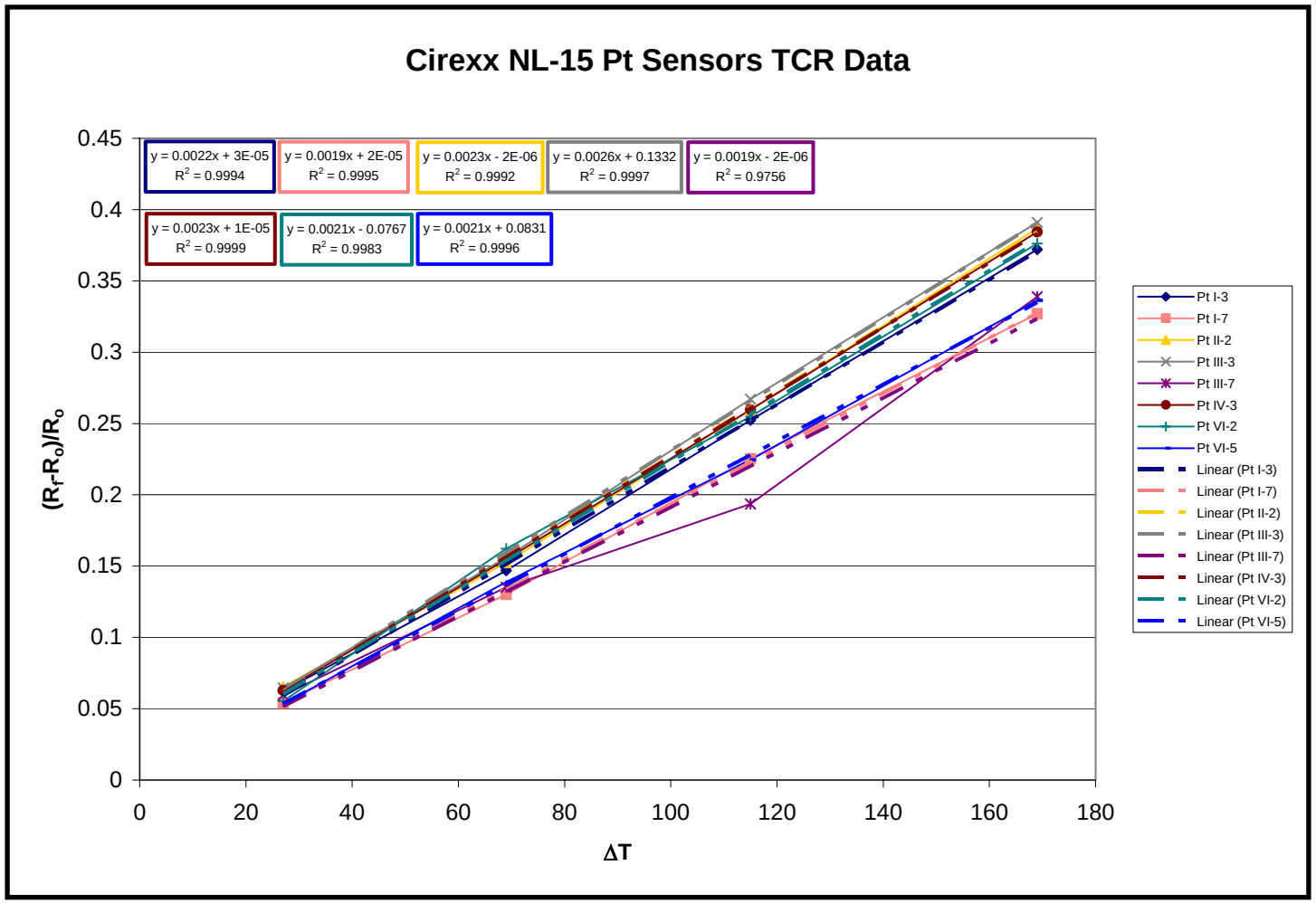

Figure 51: 2nd Generation Array NL-15 Pt Temperature Response Including TCR

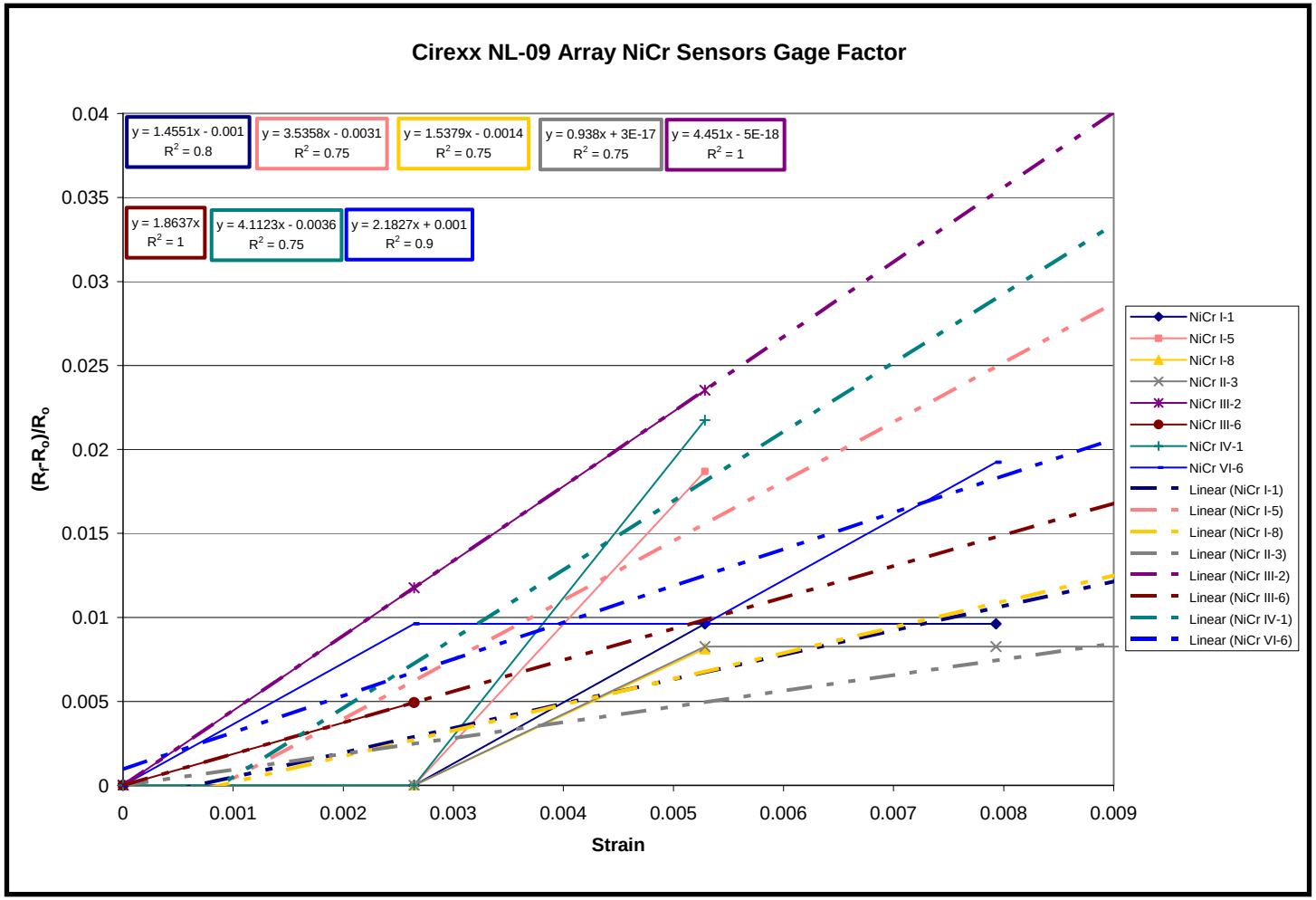

Figure 52: 2nd Generation Array NL-09 NiCr Strain Response Including Gage Factor

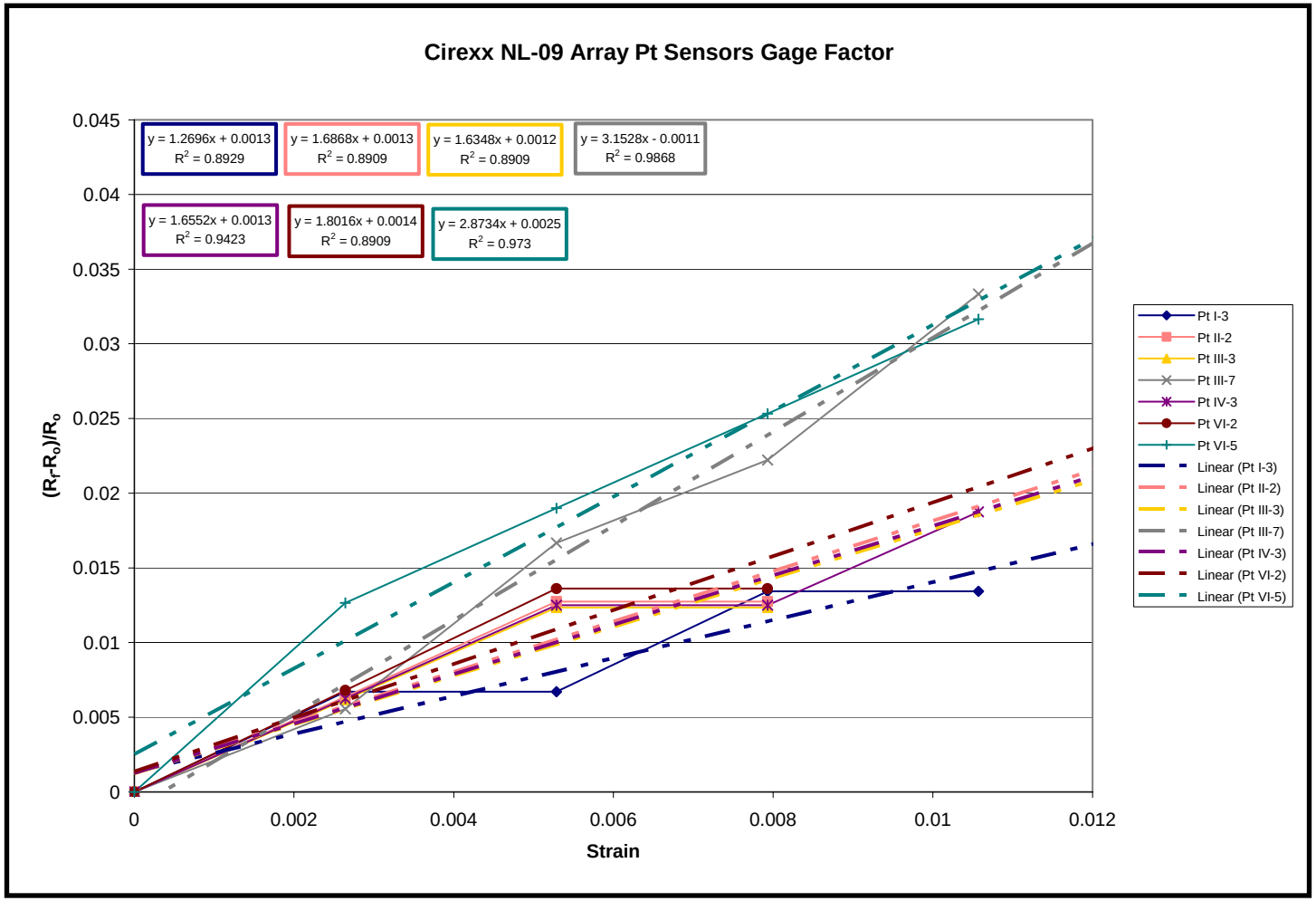

Figure 53: 2nd Generation Array NL-09 Pt Strain Response Including Gage Factor

CONCLUSIONS

This project has concluded and the results of testing of the 2nd and 3rd generation array prototypes show a consistent electrically functional sensor yield of about 25% as read from the "tail" of the sensor patch. Most sensors are not accessible due to electrical open-circuits as yet unidentified. The general design feature of sensors having different strain and temperature response has been shown, and fundamental sensor functionality has been demonstrated, in the range of RT to 180°C, and 0-1.8% strain. The summary list of accomplishments follows.

- The concept of a 3-dimensionally integrated large area strain rosette & temperature sensing arrays is both feasible and easily scalable
- Processing will require refinements
    - A 2 or 3 source magnetron is essential in allowing adhesion metal layers to be deposited without forming an oxide layer due to breaking vacuum
    - Ultra-Fine (~10nm) NiCr grain size is unacceptable for strain sensor fabrication – processing and post-processing conditions (e.g. Inert atmosphere or forming gas annealing) must promote grain growth
- Functionality has been demonstrated to ~1.8% strain
- Applications exist beyond scope of original project, e.g. flexible tiled sensor panels for wind tunnel applications

UNIQUE ASPECTS OF THE RESEARCH

- Demonstrated integrated large area flex array (6”x6”)
- Integrated Thick and Thin Film Technologies
- Integrated Large Area Anisotropic (Strain Rosette) Strain Measurement
- Novel Temperature Compensation Technique

RECOMMENDATIONS

Further testing of deposition conditions and resultant film qualities is required. It is believed that grain size and residual stresses represent the largest issues for NiChrome deposition. X-ray diffraction data of Pt shows strong (111) peaks, indicating sufficient grain size such that property problems due to small grains are unlikely. X-ray data of NiChrome shows a less well-defined peak of lower intensity, still indicating growth in the (111) plane, but not necessarily of sufficient grain size for good film properties.

Further research might be expanded to include:

- Exploration of Other Sensor Types
    - Air Flow Sensors
    - Accelerometer
- Consider Alternative Strain Sensing Materials
    - Conducting Polymer
    - Optical Fibers
        - Traditional
        - Polymer

REFERENCES

[1] Mohamad H. Hussein and George G. Goble, "A Brief History of the Application of Stress-Wave Theory to Piles" Practices and Trends in Deep Foundations 2004: Current Practices and Future Trends in Deep Foundations (GSP No. 125) Jerry A. DiMaggio, Mohamad H. Hussein, ed. July 27–July 31, 2004, Los Angeles, California

[2] http://www.omega.com/literature/transactions/volume3/strain.html Accessed on: Wednesday, May 10, 2006

[3] http://www.globalspec.com/FeaturedProducts/Detail/soltec/Triaxial_Strain_Gages_Printed_Circuit_Board_PCB/21933/0. Accessed on: Wednesday, May 10, 2006

[4] W.C. Young, R.G. Budynas, and R.J. Roarke, 'Roarke's Formulas for Stress and Strain' (7th Edition) McGraw-Hill, 81-106 (2002). Accessed on: Wednesday, May 10, 2006

[5] R.C. Hibbeler, Mechanics of Materials (3rd Edition) Prentice Hall, 500-514 (1997)

[6] Based on bulk materials properties as found in: Microchip Technology Inc., Application Note 679 (1998); www.efunda.com/designstandards/sensors (2004); and www.pelicanwire.com/nichrome80.htm (2004).

[7] C. C. Koch, "Optimization of strength and ductility in nanocrystalline and ultrafine grained metals", Acta Materialia Inc, Elsevier, 16 June 2003

[8] C.C. Koch personal conversation, April 2006.

[9] http://books.elsevier.com/us/bookscat/samples/0750664002/0750664002.pdf?mscssid=6QFV4FRBVS5P9JF1NRAL6TBHV5FA6EQ4. Accessed on: Wednesday, May 10, 2006, 1:42:08 AM

[10] T. M. Nenadovic, Z. B. Fotiric, T. S. Dimitrijevic and M. B. Adamov, "Some Characteristic Properties of Thin Films" Boris Kid& Institute of Nuclear Sciences, VinEa, 11001 Belgrade, September 14, 1971

[11] Robert E. Reed-Hill, Physical Metallurgy Principles (3rd Edition) PWS Publishing Company, Boston, 260-264 (1994)

[12] L.F. Fuller, in *Thin Film Technology Handbook*, Edited by A. Elshabini-Riad and F.D. Barlow III (McGraw-Hill, New York, 1998) 2-33.

[13] A. Elshabini and F. Barlow, in *Thin Film Technology Handbook*, Edited by A. Elshabini-Riad and F.D. Barlow III (McGraw-Hill, New York, 1998) 3-13.

[14] *Hybrid Microelectronics Handbook*, 2nd Edition, edited by J.E. Sergent and C.A. Harper (McGraw-Hill, New York, 1995), 4-13.

[15] D.M. Buczek, J. Vac. Sci. Technol. **15**(2), 370 (1978).